NAD kinase promotes *Staphylococcus aureus* pathogenesis by supporting production of virulence factors and protective enzymes

Clarisse Leseigneur[1], Laurent Boucontet[2], Magalie Duchateau[3], Javier Pizarro-Cerda[1], Mariette Matondo[3], Emma Colucci-Guyon[2], Olivier Dussurget[1]*

[1]Institut Pasteur, Université Paris Cité, CNRS UMR6047, Unité de Recherche *Yersinia*, F-75015 Paris, France ; [2]Institut Pasteur, Université Paris Cité, CNRS UMR3738, Unité Macrophages et Développement de l'Immunité, F-75015 Paris, France ; [3]Institut Pasteur, Université Paris Cité, CNRS USR2000, Unité de Spectrométrie de Masse pour la Biologie, Plateforme de protéomique, F-75015 Paris, France.

*For correspondence: olivier.dussurget@pasteur.fr

Abstract

Nicotinamide adenine dinucleotide phosphate (NADPH) is the primary electron donor for reductive reactions that are essential for the biosynthesis of major cell components in all organisms. Nicotinamide adenine dinucleotide kinase (NADK) is the only enzyme that catalyzes synthesis of NADP(H) from NAD(H). While the enzymatic properties and physiological functions of NADK have been thoroughly studied, the role of NADK in bacterial pathogenesis remains unknown. Here, we used CRISPR interference to knockdown NADK gene expression to address the role of this enzyme in *Staphylococcus aureus* pathogenic potential. We find that NADK inhibition drastically decreases mortality of zebrafish infected with *S. aureus*. Further, we show that NADK promotes *S. aureus* survival in infected macrophages by protecting bacteria from antimicrobial defense mechanisms. Proteome-wide data analysis revealed that production of major virulence associated factors is sustained by NADK. We demonstrate that NADK is required for expression of the quorum-sensing response regulator AgrA, which controls critical *S. aureus* virulence determinants. These findings support a key role for NADK in bacteria survival within innate immune cells and the host during infection.

32 **Introduction**

33 Nicotinamide adenine dinucleotide (NAD^+), its phosphorylated form ($NADP^+$) and their
34 reduced equivalents (NADH and NADPH) are essential cofactors shared by all living
35 organisms, including bacteria. While NAD^+ and NADH are important for cellular energy
36 metabolism, inflammation and senescence (Chini et al., 2021; Covarrubias et al., 2021), $NADP^+$
37 and NADPH are key cofactors in central metabolism, being involved in tricarboxylic acid
38 (TCA) cycle, pentose phosphate pathway as well as *de novo* synthesis of fatty acids, cholesterol,
39 amino acids and nucleotides (Chandel, 2021). NADPH also provides the reducing power
40 necessary for the restoration of antioxidative defense systems of the cell (Chandel, 2021). Like
41 NAD(H), growing evidence suggests that NADP(H) has a broader role. In particular, the
42 $NADP^+$ derivative nicotinic acid adenine dinucleotide phosphate (NAADP), which is the major
43 intracellular calcium mobilizing molecule, links NADP(H) metabolism with calcium
44 homeostasis and signaling, development and differentiation (Galione and Chuang, 2020).

45 Whereas there are two known multi-step pathways for NAD^+ biosynthesis, a single
46 enzyme is responsible for the phosphorylation of NAD^+/NADH into $NADP^+$/NADPH: the
47 NAD kinase (NADK) (McGuinness and Butler, 1985; Chini et al., 2021). NADK activity was
48 first reported in the late 30's (Vestin, 1937; Von Euler and Adler, 1938), and the enzyme was
49 purified from yeast by Kornberg in 1950 (Kornberg, 1950). It is only in 2000 that the genes
50 encoding NADK were identified in *Micrococcus flavus* and *Mycobacterium tuberculosis*
51 (Kawai et al., 2000). Since then, NADK genes have been identified in all living organisms,
52 except the intracellular parasitic bacteria *Chlamydia* spp. on the basis of genome annotation
53 (Grose et al., 2006; Fisher et al. 2013). Given the vital role of NADPH, notably during oxidative
54 stress, NADK genes have been shown to be essential for growth of several bacteria, such as
55 *Mycobacterium tuberculosis* (Sassetti et al., 2003), *Bacillus subtilis* (Kobayashi et al., 2003),
56 *Salmonella enterica* (Grose et al., 2006) and *Staphylococcus aureus* (Chaudhuri et al., 2009;

57 Gelin et al., 2020). NADKs essentiality may account for the poor characterization of their role
58 in prokaryotes. In contrast, NADKs have been extensively studied in plants (Li et al., 2018),
59 especially in *Arabidopsis thaliana* which possesses three NADK encoding genes (Chai et al.,
60 2006; Turner et al., 2004). NADK has a key role in photosynthesis, plant cell metabolism,
61 intracellular redox balance (Li, 2018), and response to stresses as shown during exposure to
62 aluminum in wheat (Ślaski, 1995), upon cold-shock in green bean leaves (Ruiz et al., 2002),
63 upon treatment with NaCl, ionizing radiations or oxidative stress in *Arabidopsis thaliana* (Chai
64 et al., 2006; Berrin et al., 2005). In plants, NADKs are regulated by calcium and calmodulin
65 (Tai et al., 2019). In contrast, in prokaryotes allosteric regulation of NADK activity by NADPH
66 or NADH is the main mechanism identified so far (Grose et al., 2006).

67 The importance of microbial metabolic adaptation during infection (Eisenreich et al.,
68 2010; Richardson, 2019; Teoh et al., 2021) and the unknown contribution of NADK to bacterial
69 pathogenesis prompted us to investigate the role of NADK in *Staphylococcus aureus*
70 pathogeny. While being carried as a commensal by around one third of the human population,
71 *S. aureus* is a leading cause of infectious diseases, ranging from mild skin and soft tissue
72 infections to life-threatening endocarditis and bacteremia (Turner et al., 2019). Worryingly, *S.*
73 *aureus* can develop resistance to virtually all antibiotic classes available (Vestergaard et al.,
74 2019), limiting dramatically therapeutic options for some patients. Therefore, WHO included
75 *S. aureus* in the list of high priority pathogens to promote research and development of new
76 antibiotics and emphasized the need for innovation and diversification in the choice of targets
77 (https://www.who.int/news/item/27-02-2017-who-publishes-list-of-bacteria-for-which-new-
78 antibiotics-are-urgently-needed).

79 In this study, we used a genetic approach to modulate NADK activity and analyze *S.*
80 *aureus* behavior in the infected host, in infected cells and in response to stresses mimicking
81 those encountered during infection. We establish the first link between NADK activity and *S.*

82 *aureus* pathogenic potential, as NADK inhibition led to an increased survival of the host in a
83 zebrafish infection model. We further demonstrate that inhibition of NADK leads to a dramatic
84 decrease of *S. aureus* survival in macrophages, highlighting the enzyme importance during
85 interactions with immune cells. We further show that exposures to oxidative and envelope-
86 targeting antimicrobial compounds significantly decrease bacterial survival upon inhibition of
87 NADK activity. Proteomic analysis indicated that the production of protective enzymes,
88 virulence factors and the quorum-sensing response regulator AgrA relies on NADK. Thus, our
89 results reveal a key role for NADK in bacterial pathogenesis.

90 ## Results

91 **NADK contributes to *S. aureus* virulence in zebrafish**

92 As most prokaryotes, *S. aureus* possesses a single NADK encoded by the highly conserved
93 *ppnK* gene. To investigate the role of NADK in *S. aureus* pathogenesis, we followed a genetic
94 approach to modulate the expression of *ppnK*. We used the *S. aureus* NADK sgRNA strain
95 (Gelin et al., 2020), in which the levels of *ppnK* expression were decreased by CRISPR
96 interference based on plasmid pSD1 (Zhao et al., 2017). Knockdown of NADK expression in
97 this strain was analyzed by RT-PCR, immunoblotting, and aerobic growth in BHI at 37°C
98 (Figure supplement 1). Growth of the *S. aureus*/sgRNA strain was affected as previously
99 reported (Gelin et al., 2020), attesting the efficiency of the knockdown. We investigated
100 whether NADK inhibition might influence *S. aureus* pathogenesis in a zebrafish infection
101 model. This model allows short kinetics of infection (Prajsnar et al., 2008) and has been
102 previously used to study *S. aureus* infection dynamics (Prajsnar et al., 2012). In addition to
103 being optically transparent, zebrafish larvae innate immune system is the only one operating
104 during the first days of development, facilitating the study of interactions between bacteria and
105 neutrophils or macrophages. We first determined the stability of the pSD1 plasmid during
106 infection. Zebrafish larvae were infected at 60 hours post fertilization (hpf) by intravenous
107 injections of either *S. aureus* containing the empty vector pSD1 or the knockdown NADK
108 sgRNA strain. Bacteria recovered from infected larvae were plated onto BHI agar with and
109 without chloramphenicol. There was no significant difference between the number of bacteria
110 growing on BHI alone and BHI supplemented with chloramphenicol up to 48 hours post-
111 infection (hpi), irrespective of the strain (Figure supplement 2A). Thus, plasmids were
112 maintained in our experimental infection conditions. We next monitored zebrafish survival
113 upon infection with 10^4 bacteria. *S. aureus*/pSD1 infection led to ≈ 75% fish mortality at 24 hpi
114 (Figure 1A). Strikingly, only one larva out of 48 died when bacterial NADK was inhibited

115 (Figure 1A). Decreased fish mortality upon *S. aureus*/NADK sgRNA infection was also
116 observed 48 and 72 hpi (Figure 1A). These results indicate that NADK inhibition leads to a
117 decreased bacterial virulence. We then determined the bacterial burden of fish larvae 24 and 48
118 hpi. Interestingly, numbers of *S. aureus*/pSD1 and *S. aureus*/NADK sgRNA bacteria at both
119 time points varied depending on the viability of the fish (Figure 1B). As observed previously
120 by Prasjnar et al. (Prajsnar et al., 2012), some fishes were able to control the infection with 10^4
121 bacteria but a high bacterial burden was associated with larval death in most cases (Figure 1B).
122 Early mortality was observed in zebrafish in which *S. aureus*/pSD1 developed to high numbers
123 compared to larvae infected with the NADK knockdown strain. Together, these results suggest
124 that NADK contributes to *S. aureus* pathogenic potential, which depends on both bacterial and
125 host factors. To investigate the impact of NADK inhibition on phagocyte populations, we
126 infected intravenously transgenic zebrafish lines with *S. aureus*/pSD1 or *S. aureus*/NADK
127 sgRNA strains, and observed bacteria, macrophages and neutrophils at time 0, 6, 12 and 24 hpi.
128 *S. aureus*/pSD1 bacterial burden was higher than that of *S. aureus*/NADK sgRNA strain in head
129 and caudal regions observed in fish of comparable viability 12 hours (Figure 1C) and 24 hpi
130 (Figure supplement 2B). We also noticed a strong depletion of neutrophils in larvae infected
131 with *S. aureus*/pSD1, while this neutropenia was more limited upon infection with NADK
132 knockdown bacteria (Figures 1C, 1D and 1E). This correlated with virulence differences of the
133 two strains, given the key role of neutrophils in *S. aureus* infection (Pollitt et al., 2018; Prajsnar
134 et al., 2012). In contrast, the number of macrophages in larvae did not significantly decreased
135 upon infection with either strains (Figure supplement 2C). Altogether, our results suggest that
136 NADK is important for *S. aureus* pathogenesis.

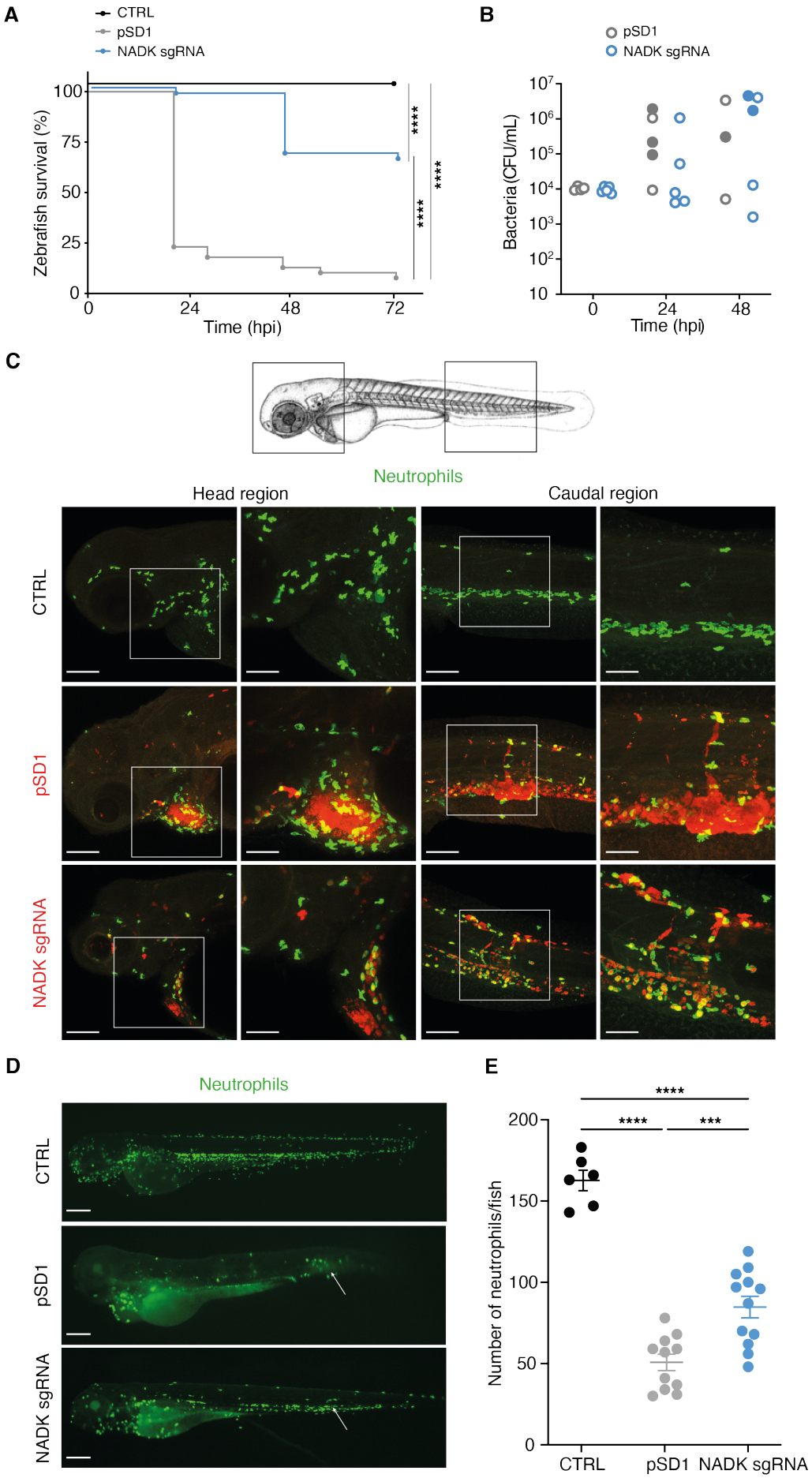
A
CTRL
pSD1
NADK sgRNA
Zebrafish survival (%)
100
75
50
25
0
0
24
48
72
Time (hpi)
****
****
****
B
pSD1
NADK sgRNA
Bacteria (CFU/mL)
10^7
10^6
10^5
10^4
10^3
10^2
10
0
24
48
Time (hpi)
C
Neutrophils
Head region
Caudal region
CTRL
pSD1
NADK sgRNA
D
Neutrophils
CTRL
pSD1
NADK sgRNA
E
****
****
***
Number of neutrophils/fish
200
150
100
50
0
CTRL
pSD1
NADK sgRNA

138 **Figure 1** NADK promotes *S. aureus* virulence in zebrafish. (A) Survival of zebrafish larvae uninfected (CTRL)
139 or intravenously injected at 60 hpf with 10^4 *S. aureus* containing the empty vector (pSD1) or the NADK
140 knockdown strain (NADK sgRNA) between 0 and 72 hpi (n=48). (B) Bacterial burden in zebrafish larvae upon
141 intravenous injection with 10^4 *S. aureus* containing the empty vector (pSD1) or the NADK knockdown strain
142 (NADK sgRNA). For each strain, CFU were determined in living larvae (open circles) or dead larvae (filled
143 circles) 0, 24 and 48 hpi. (C) Representative fluorescence confocal images of transgenic *mpx:GFP* zebrafish larvae
144 uninfected (CTRL), or intravenously injected with 10^4 *S. aureus* containing the empty vector (pSD1) or the NADK
145 knockdown strain (NADK sgRNA) at 12 hpi. Maximum intensity Z-projection images (2-µm serial optical
146 sections) of bacteria (red) and neutrophils (green). Scale bars, 25 µm. Insets are shown at higher magnification on
147 the right panels for head and caudal regions. Scale bars, 10 µm. Neutrophils containing NADK knockdown
148 bacteria can be seen in the caudal inset. (D) Representative fluorescence confocal images of transgenic *mpx:GFP*
149 zebrafish larvae uninfected (CTRL), or intravenously injected with 10^4 *S. aureus* containing the empty vector
150 (pSD1) or the NADK knockdown strain (NADK sgRNA) at 24 hpi, showing neutrophils (green). White arrows
151 indicate the injection site. Scale bars, 500 µm (E) Number of neutrophils in uninfected zebrafish larvae (CTRL)
152 or in zebrafish larvae intravenously injected with 10^4 *S. aureus* containing the empty vector (pSD1) or the NADK
153 knockdown strain (NADK sgRNA) at 24 hpi. Comparison of data was performed using one-way analysis of
154 variance (***$p<0.001$, ****$p<0.0001$).
155

156 **NADK promotes *S. aureus* survival in macrophages**

157 Since both neutrophils and macrophages are key immune cells specialized in the destruction of
158 microorganisms, we next investigated if, in addition to triggering neutrophil killing, NADK
159 might support *S. aureus* survival during macrophages infection. Murine RAW264.7
160 macrophages were infected with *S. aureus*/pSD1 or *S. aureus*/NADK sgRNA strains. Bacterial
161 enumerations were performed at time zero and at 1, 2, 4 and 6 hpi. No significant difference in
162 initial phagocytosis of the two strains could be observed, nor at early time of infection (Figure
163 2A). In contrast, after 2 hours of infection the percentage of intracellular bacteria was
164 significantly reduced upon *ppnK* knockdown, and the survival defect increased over time
165 (Figure 2A), indicating that bacteria were not able to survive inside macrophages without

166 proper NADK activity. As oxidative burst is a major antimicrobial mechanism of phagocytes
167 (Fang, 2004), we next investigated the role of ROS produced by macrophages in the control of
168 the *S. aureus*/NADK sgRNA strain using the antioxidant agent N-acetyl cysteine (NAC). NAC
169 partially restored bacterial survival (Figure 2A), indicating that the bacterial growth defect of
170 the *ppnK* knockdown strain was due to its inability to cope with oxidative stress to some extent.
171 Using confocal fluorescence microscopy, we then investigated bacterial intracellular
172 localization in macrophages 6 hours post-infection. Few *S. aureus*/NADK sgRNA bacteria were
173 detected compared to *S. aureus*/pSD1 (Figure 2B), and NAC treatment led to an increased
174 number of bacteria (Figure 2C), confirming bacterial enumeration results. Interestingly, while
175 all knockdown bacteria colocalized with lysosomal associated membrane protein 1 (LAMP1),
176 many *S. aureus*/pSD1 did not upon NAC treatment, suggesting that NADK activity might be
177 required for phagolysosome escape and bacterial survival in macrophages. Since *S. aureus* has
178 been shown to be cytotoxic to macrophages, we next wondered if the bacterial growth defect
179 of the NADK knockdown strain was correlated with reduced lysis of infected cells. We
180 measured the levels of cell death in macrophages that were uninfected, uninfected and treated
181 with Triton X-100 or infected with *S. aureus*/pSD1 or *S. aureus*/NADK sgRNA strains.
182 Detergent treatment expectedly led to massive cell lysis. Infections produced significant
183 macrophage death compared to uninfected cells, although to much lower levels than that
184 triggered by Triton X-100. Infection with the *ppnK* knockdown strain was significantly less
185 cytotoxic than infection with the *S. aureus*/pSD1 strain. Altogether, these results suggest than
186 NADK promotes survival and possibly virulence of *S. aureus* in macrophages.

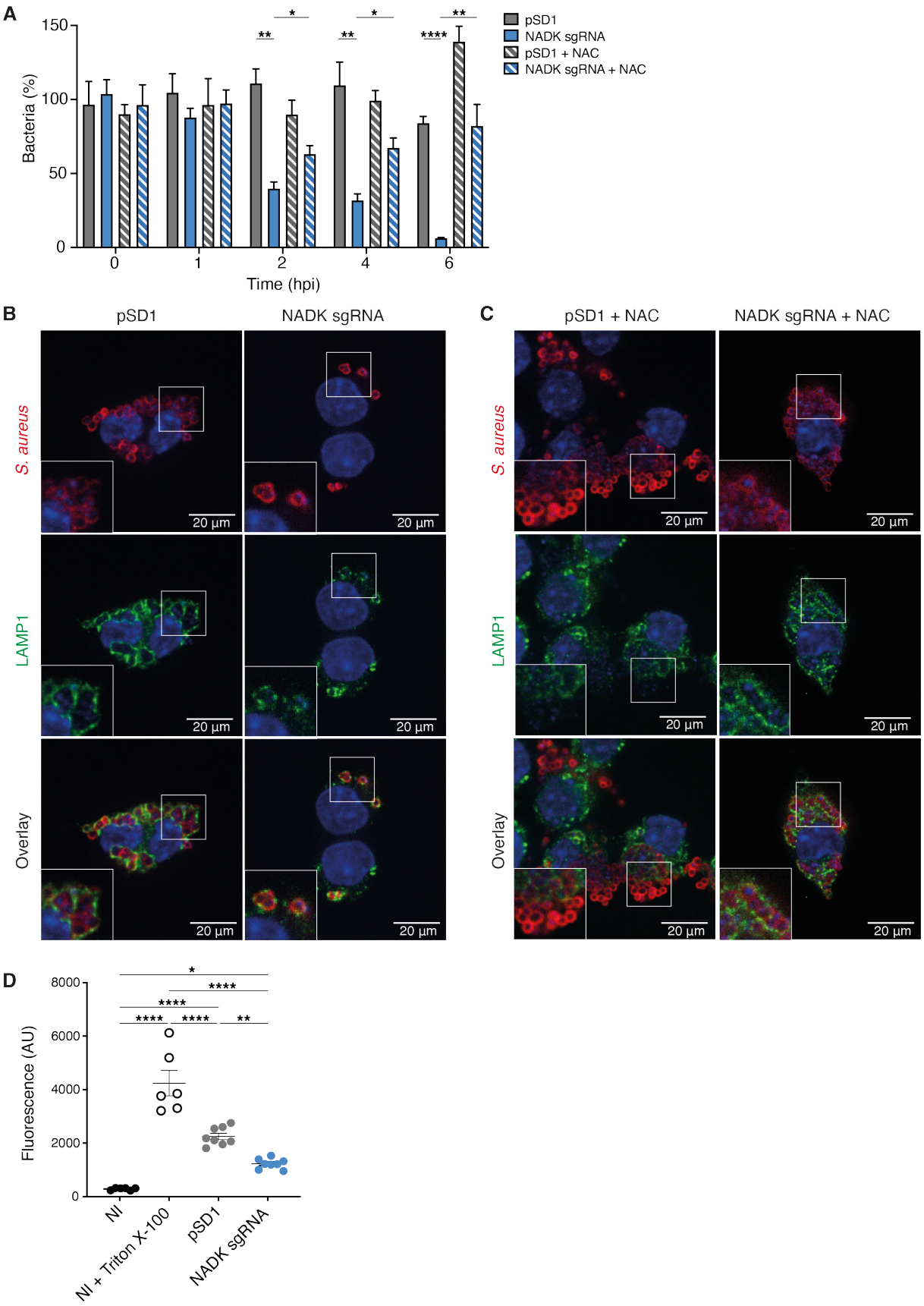
A
Bacteria (%)
150
100
50
0
0
1
2
4
6
Time (hpi)
pSD1
NADK sgRNA
pSD1 + NAC
NADK sgRNA + NAC
B
pSD1
NADK sgRNA
S. aureus
LAMP1
Overlay
20 µm
C
pSD1 + NAC
NADK sgRNA + NAC
D
Fluorescence (AU)
8000
6000
4000
2000
0
NI
NI + Triton X-100
pSD1
NADK sgRNA

189 **Figure 2** NADK promotes *S. aureus* survival and cytotoxicity in macrophages. (A) Percentage of growth of the *S.*
190 *aureus* strains containing the empty vector (pSD1) or the *ppnK* knockdown strain (NADK sgRNA) at time 0, and
191 1, 2, 4 and 6 hpi of RAW264.7 macrophages left untreated or treated with N-acetylcysteine (NAC). Bars indicate
192 standard errors of the means of biological replicates (n=4). Comparison of data was performed using two-ways
193 analysis of variance (*p<0.05, **p<0.01, ****p<0.0001). (B-C) Representative images of RAW264.7
194 macrophages infected with *S. aureus*/pSD1 or *S. aureus*/NADK sgRNA strains and analyzed 6 hpi by confocal
195 fluorescence microscopy using antibodies to label *S. aureus* (Cy5, red) and LAMP-1 (FITC, green). Nuclei were
196 labeled with DAPI (blue). B shows untreated macrophages. C shows macrophages treated with NAC. Insets are
197 shown at higher magnification. Images are representative of three independent experiments. (D) Cell death of
198 RAW264.7 macrophages uninfected (NI), uninfected and treated with Triton X-100 (lysis control), or 6 hpi with
199 *S. aureus* strains containing the empty vector (pSD1) or the *ppnK* knockdown strain (NADK sgRNA). Bars
200 indicate standard errors of the means of biological replicates. Comparison of data was performed using two-ways
201 analysis of variance (*p<0.05, **p<0.01, ****p<0.0001). Data are representative of at least three independent
202 experiments.
203
204 **NADK protects *S. aureus* from antimicrobial defense compounds**
205 Hydrogen peroxide is one of the reactive oxygen species generated upon activation of
206 macrophages (Fang, 2004). We therefore compared growth of the *S. aureus* strain containing
207 the empty vector to that of the NADK knockdown strain, upon exposure to increasing
208 concentrations of hydrogen peroxide (H_2O_2). While the *S. aureus*/pSD1 strain resisted to high
209 doses of H_2O_2, the *S. aureus*/NADK sgRNA strain showed increasing growth deficiency when
210 exposed to H_2O_2 concentrations ranging from 50 to 500 μM H_2O_2 (Figure 3A). Expectedly,
211 treatment of the *S. aureus*/pSD1 strain with catalase alone or catalase and H_2O_2 did not affect
212 growth (Figure 3B). In contrast, addition of catalase, which catalyzes hydrogen peroxide
213 dismutation into water and oxygen, rescued the growth defect of the *S. aureus*/NADK sgRNA
214 strain upon H_2O_2 treatment (Figure 3B). Taken together, our results show that NADK protects
215 *S. aureus* from toxic effects of a reactive oxygen species involved in host defense. Within
216 phagocytes, bacteria have to cope with other mechanisms of antimicrobial defenses such as

217 production of lysozyme (Callewaert and Michiels, 2010; Avican et al., 2021; Fang et al., 2016).
218 We thus investigated the effects of NADK knockdown on *S. aureus* sensitivity to lysozyme.
219 Since *S. aureus* is highly resistant to lysozyme, we treated bacteria with lysozyme and the
220 bacteriocin lysostaphin, a combination which potentiates their antibacterial activity against *S.*
221 *aureus* (Cisani et al., 1982). At subinhibitory concentrations for the *S. aureus*/pSD1 strain, the
222 *S. aureus*/NADK sgRNA strain showed decreased viability when exposed to lysozyme and
223 lysostaphin (Figure 3C). Thus, NADK protects *S. aureus* from toxic effects of cell envelope-
224 targeting compounds.

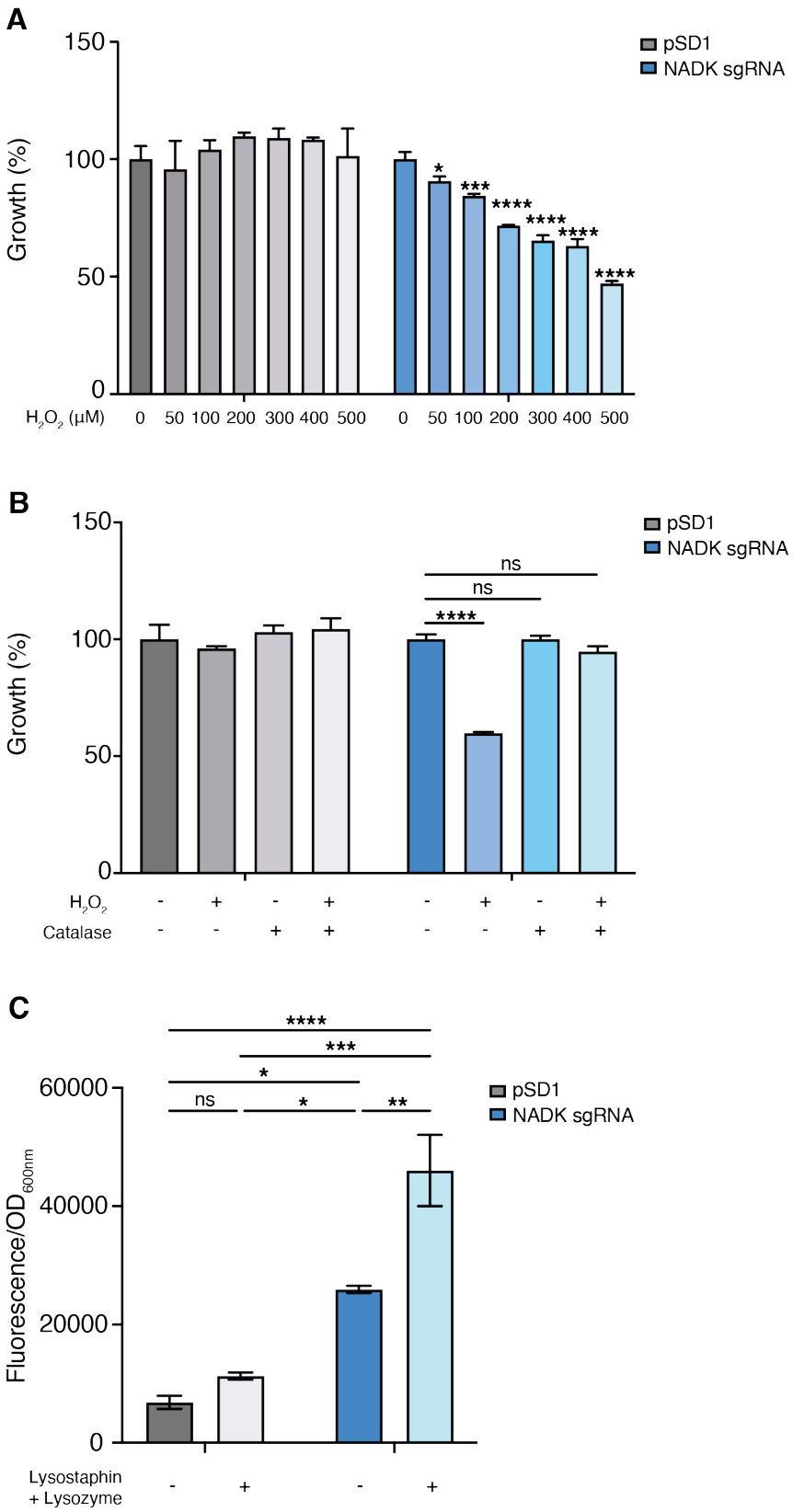
A
150
100
50
0
Growth (%)
pSD1
NADK sgRNA
*
***
****
****
****
****
H2O2 (μM)
0 50 100 200 300 400 500 0 50 100 200 300 400 500
B
150
100
50
0
Growth (%)
pSD1
NADK sgRNA
ns
ns
****
H2O2
Catalase
C
****
***
*
ns
*
**
60000
40000
20000
0
Fluorescence/OD600nm
pSD1
NADK sgRNA
Lysostaphin
+ Lysozyme

225

226

227

228 **Figure 3** NADK protects *S. aureus* from antimicrobial defense compounds. Bacterial growth was monitored at
229 OD_{600nm} in BHI broth at 37°C. (A) Percentage of growth of the *S. aureus* strain containing the empty vector (pSD1)
230 and the *ppnK* knockdown strain (NADK sgRNA) exposed for 6 hours to increasing concentrations of H_2O_2 relative
231 to the untreated condition. (B) Percentage of growth of the *S. aureus* strain containing the empty vector (pSD1)
232 and the *ppnK* knockdown strain (NADK sgRNA) exposed for 6 hours to H_2O_2 and catalase alone or in combination,
233 relative to the untreated condition. Data shown are representative of three independent experiments. Bars indicate
234 the standard error of the means of biological replicates. Comparison of data was performed using one-way analysis
235 of variance (ns: nonsignificant, *p<0.05, ***p<0.001, ****p<0.0001). (C) Bacterial cell death of the *S. aureus*
236 strain containing the empty vector (pSD1) and the *ppnK* knockdown strain (NADK sgRNA) untreated or exposed
237 for 30 min to 0.05 mg/mL lysostaphin and 5 mg/mL lysozyme. Bacterial permeability was assessed using the
238 CellTox Green cytotoxicity assay. Bars indicate standard errors of the means of biological replicates. Comparison
239 of data was performed using two-ways analysis of variance (*p<0.05, **p<0.01, ***p<0.001, ****p<0.0001).
240 Data are representative of at least three independent experiments.
241

242 **NADK supports *S. aureus* protective enzymes**

243 To elucidate mechanisms of action of NADK, unbiased mass spectrometry-based proteomics
244 was used to identify proteins differentially expressed upon NADK knockdown. Relative protein
245 abundance was compared in the *S. aureus* strain containing the empty vector and the NADK
246 knockdown strain grown in BHI. Interestingly, lower levels of major antioxidant enzymes were
247 detected in the NADK sgRNA strain (Table 1 and table supplement 1). NADK deficiency was
248 linked to decreased relative abundance of superoxide dismutase SodM, catalase KatA,
249 thioredoxin Trx2 and methionine sulfoxide reductase MsrA2. Additionally, the NADK sgRNA
250 strain had lower levels of the peptidoglycan *O*-acetyltransferase OatA and the glycopeptide
251 resistance-associated two-component system GraRS, major determinants for *S. aureus*
252 resistance to lysozyme and cationic antimicrobial peptides (CAMP), respectively (Bera et al.,
253 2005 ; Herbert et al., 2007). We then compared the proteomes of the *S. aureus* strain containing
254 the empty vector and the NADK knockdown strain upon hydrogen peroxide treatment. OatA,
255 SodM, Trx2, MrsA2, KatA and other antioxidant enzymes were more abundant in the *S.*

256 *aureus*/pSD1 strain than in the NADK deficient strain (Table supplement 2 and table
257 supplement 3), as it had been observed when strains were grown in BHI. To determine the
258 effect of NADK knockdown on *S. aureus* proteome *in vivo*, relative protein abundance was
259 analyzed in zebrafish infected with the *S. aureus* strain containing the empty vector or the
260 NADK knockdown strain. The D-alanyl carrier protein DltC, which mediates CAMP
261 resistance, and antioxidant enzymes, such as SodA, KatA, thiol peroxidase Tpx and alkyl
262 hydroperoxide reductase subunit AhpF, were detected in zebrafish infected with *S.*
263 *aureus*/pSD1 (Tables S4 and S5). In contrast, these proteins were undetectable in *S.*
264 *aureus*/NADK sgRNA-infected zebrafish. Thus, our approach identified a role for NADK in
265 supporting *S. aureus* protective proteins *in vitro* and *in vivo*.
266
267 **Table 1.** Relative abundance of a subset of protective proteins differentially expressed by *S.*
268 *aureus* pSD1 and NADK sgRNA strains.
269

Uniprot	Protein	Description	Log2R*	P**
Q2FV54	OatA	O-acetyl transferase	3.07	1.78E-05
Q2G000	Trx2	Thioredoxin 2	1.79	2.75E-05
Q2G261	SodM	Superoxide dismutase [Mn/Fe]	1.68	2.11E-06
Q2FZZ3	-	Thioredoxin domain-containing protein	1.59	7.22E-04
Q2G0D9	GraS	Sensor histidine kinase	1.31	4.00E-04
Q2G280	-	Peroxiredoxin	1.26	6.69E-07
P0A086	MsrA2	Methionine sulfoxide reductase	1.10	2.25E-05
Q2FVL7	-	Thioredoxin domain-containing protein	1.02	1.94E-03
Q2G0E0	GraR	Response regulator protein	1.00	2.23E-03
Q2FYU7	KatA	Catalase	0.59	1.00E-05

270
271 * Log2R=Log2[pSD1]/[NADK sgRNA]
272 **Adjusted p value
273
274
275 **NADK promotes virulence factor expression by *S. aureus***
276 To investigate additional mechanisms of action of NADK, our quantitative proteomic data were
277 analyzed further using proteomaps (Liebermeister et al., 2014). *S. aureus* proteins were
278 classified into functional groups based on KEGG annotation. Expression profiles of strains

279 grown in BHI were visualized by Voronoi tree maps, clustering proteins in three hierarchical
280 categories. Top-level functional categories relying on NADK activity included biosynthesis,
281 central carbon metabolism, other enzymes, folding, sorting and degradation, translation,
282 transcription, and DNA maintenance (Figure 4A). Remarkably, infectious diseases, signaling
283 molecules and interaction, and signal transduction identified at the highest level (Figure 4A),
284 and *Staphylococcus aureus* infection, bacterial toxins and two-component system identified at
285 the second level (Figure 4B), encompassed multiple major virulence factors such as alpha-
286 hemolysin, gamma-hemolysin, Map, IsdA, and virulence regulators AgrA and SaeS (Figure
287 4C). NADK deficiency was also linked to decreased relative abundance of other virulence-
288 related proteins, *e.g.,* phenol-soluble modulin (PSM) alpha PsmA, the lipase Lip1, leukocidin-
289 like proteins 1 and 2, and staphopain A (Table 2). Of note, similar proteomic profiles were
290 obtained when strains were exposed to hydrogen peroxide, confirming the importance of
291 NADK for proper expression of virulence proteins in conditions mimicking host defenses
292 (Figure supplement 3, Table supplement 6). Furthermore, comparative analysis of whole
293 protein extracts from bacterial pellets and culture supernatants by immunoblotting showed a
294 massive decrease in the levels of alpha-hemolysin secretion by the NADK deficient strain
295 (Figures 4D and 4E). To determine if the differential protein abundance of toxins was translated
296 into different levels of enzymatic activity, a Christie-Atkins-Munch-Peterson test was
297 performed using *S. aureus* RN4220, *S.aureus*/pSD1, and *S. aureus*/NADK sgRNA strains
298 (Adhikari et al. 2007). Strikingly, NADK deficiency led to a lack of hemolysis (Figure 4F). In
299 contrast *S. aureus*/pSD1 produced a synergistic hemolysis in presence of the RN4220 strain,
300 indicating secretion of hemolysins and phenol soluble modulins. Taken together, these data
301 suggest that NADK is required for expression of *S. aureus* virulence determinants.
302

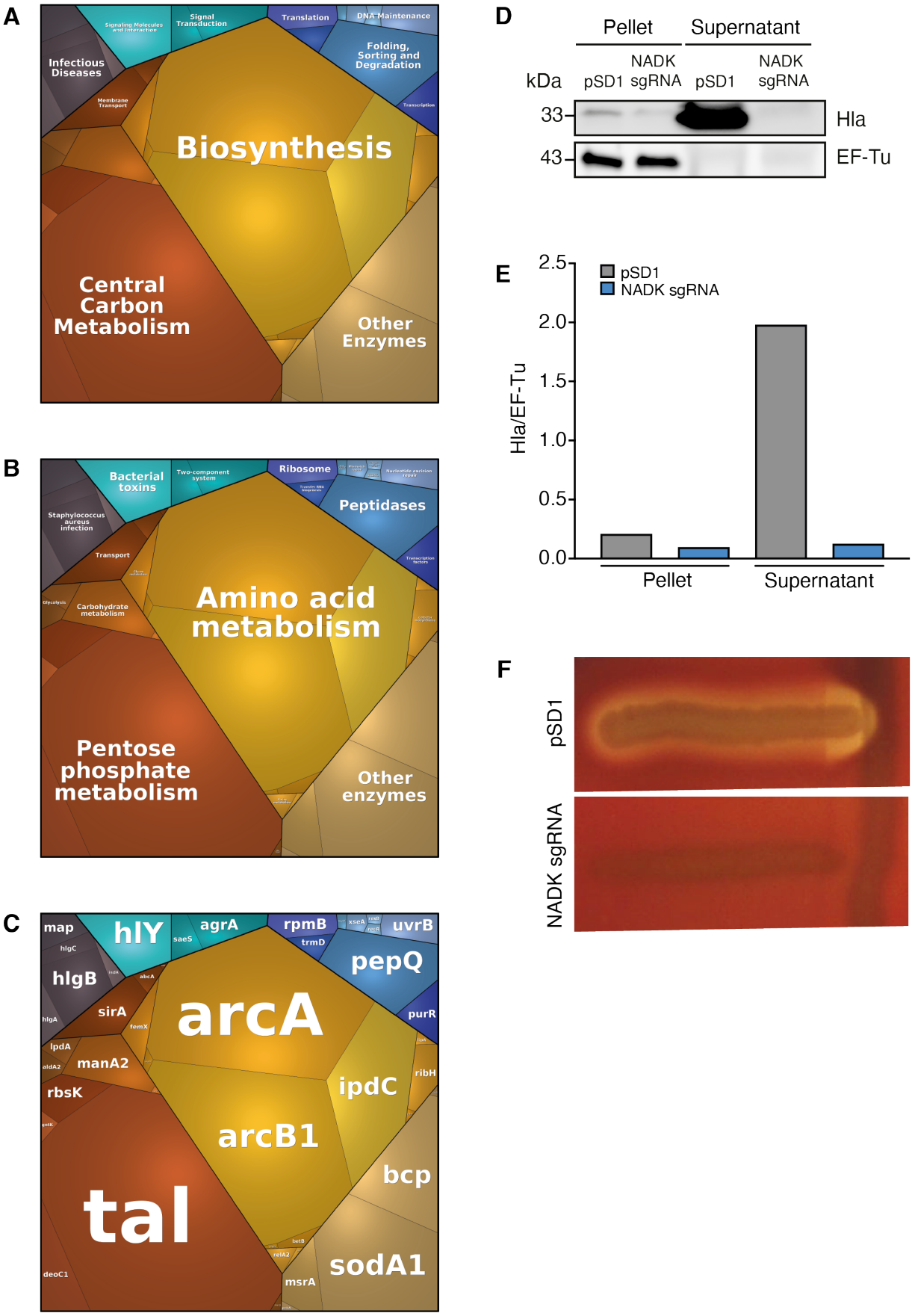
A
Signaling Molecules and Interaction
Signal Transduction
Translation
DNA Maintenance
Infectious Diseases
Folding, Sorting and Degradation
Membrane Transport
Transcription
Biosynthesis
Central Carbon Metabolism
Other Enzymes
B
Bacterial toxins
Two-component system
Ribosome
Nucleotide excision repair
Peptidases
Staphylococcus aureus infection
Transport
Transcription factors
Glycolysis
Carbohydrate metabolism
Amino acid metabolism
Pentose phosphate metabolism
Other enzymes
C
map
hlY
agrA
rpmB
xseA
uvrB
hlgC
saeS
trmD
pepQ
hlgB
abcA
sirA
arcA
purR
hlgA
femX
lpdA
aldA2
manA2
ribH
rbsK
ipdC
arcB1
bcp
tal
betB
relA2
sodA1
deoC1
msrA
D
Pellet
Supernatant
kDa
pSD1
NADK sgRNA
pSD1
NADK sgRNA
33
43
Hla
EF-Tu
E
pSD1
NADK sgRNA
Hla/EF-Tu
2.5
2.0
1.5
1.0
0.5
0.0
Pellet
Supernatant
F
pSD1
NADK sgRNA

303

304 **Figure 4** NADK promotes expression of *S. aureus* virulence determinants. The *S. aureus* strain containing the
305 empty vector (pSD1) and the *ppnK* knockdown strain (NADK sgRNA) were grown in BHI broth at 37°C. (A-C)
306 Whole bacterial cell lysates were analyzed by LC-MS/MS. Voronoi treemaps were generated to visualize proteins
307 more abundant in *S. aureus*/pSD1 than in the knockdown strain at three hierarchical levels according to KEGG
308 database: top level (A), second level (B), third level (C). Colors represent functional categories. Category size
309 based on LFQ intensity corresponds to differences in protein abundance. (D) Whole bacterial cell lysates and
310 culture supernatants were analyzed by immunoblotting using antibodies against alpha-hemolysin and EF-Tu. (E)
311 Quantification of the Hla immunoblots normalized to corresponding EF-Tu protein levels in the pellet. (F) A
312 Christie-Atkins-Munch-Peterson test was performed by streaking the *S. aureus* strain containing the empty vector
313 (pSD1) and the *ppnK* knockdown strain (NADK sgRNA) perpendicularly to the *S. aureus* RN4220 strain that
314 produces only beta-hemolysin (vertical streak) on sheep blood agar. Clearing zones indicate hemolysis.

315

316 **Table 2.** Relative abundance of a subset of virulence-related proteins differentially expressed
317 by *S. aureus* pSD1 and NADK sgRNA strains.
318

Uniprot	Protein	Description	Log2R*	P**
Q2FWM4	AgrA	Accessory gene regulator protein	+	NA
P0C818	PsmA4	Phenol-soluble modulin alpha 4	+	NA
Q2FVK2	HlgC	Gamma-hemolysin component C	+	NA
P0C7Y1	PsmA1	Phenol-soluble modulin alpha 1	+	NA
Q2FUU5	Lip1	Lipase	+	NA
Q2FVK1	HlgB	Gamma-hemolysin component B	7.88	3.85E-10
Q2G1X0	Hly	Alpha-hemolysin	6.99	3.85E-10
Q2FWN9	LukL2	Leukocidin-like protein 2	3.88	4.14E-08
Q2FVK3	HlgA	Gamma-hemolysin component A	3.84	1.47E-08
Q2FWP0	LukL1	Leukocidin-like protein 1	3.09	2.25E-06
Q2G2R8	SspP	Staphopain A	2.89	4.08E-07

319
320 *Log2R=Log2[pSD1]/[NADK sgRNA]; +: protein detected in pSD1 strain and not detected from NADK sgRNA strain
321 **Adjusted p value: NA: not applicable
322

323

324 **NADK promotes AgrA expression by *S. aureus***

325 AgrA is a central regulator of *S. aureus* virulon. Therefore, the impact of NADK on AgrA
326 observed above may account for the positive regulation of virulence factor production. To attest
327 NADK-dependent regulation of virulence determinants controlled by Agr, we analyzed
328 transcript levels of two additional members of the Agr regulon, the positively regulated

329 multifunctional RNA RNAIII and the negatively regulated glutathione peroxidase gene *bsaA*.
330 We carried out RT-PCR on RNA purified from the *S. aureus* strain containing the empty vector
331 and the NADK knockdown strain during exponential growth in BHI broth at 37°C. Decreased
332 RNAIII transcript levels and increased *bsaA* transcript levels were detected in the NADK
333 knockdown strain (Figures 5A, 5B and 5D). These results are in accordance with the positive
334 regulatory role of NADK on AgrA, and the regulation of AgrA on RNAIII and *bsaA* expression.
335 To determine whether NADK sustains AgrA protein levels by promoting gene expression,
336 AgrA transcript levels were compared in the *S. aureus*/pSD1 and *S. aureus*/NADK sgRNA
337 strains. The expression of *agrA* was strongly decreased upon NADK knockdown (Figures 5C
338 and 5D). Thus, full NADK activity is required for optimal *agrA* expression and subsequent
339 virulence gene expression. To decipher the mode of action of NADK on *agrA* expression, we
340 next investigated the effect of the *ppnK* knockdown on *S. aureus* oxidative content, since
341 transcription of the *agr* system is repressed in oxidizing conditions (Baker et al., 2010; Rothfork
342 et al., 2004). We compared the levels of ROS in the *S. aureus*/pSD1 and NADK sgRNA strains
343 grown in aerobic conditions. Decreasing NADK levels led to a significant increase in ROS
344 content (Figure 5E), which could contribute to negative regulation of AgrA expression.
345 Together, our data suggest that NADK activity is important for proper *agrA* expression,
346 possibly by controlling the bacterial redox state, ultimately promoting *S. aureus* virulence
347 potential.
348

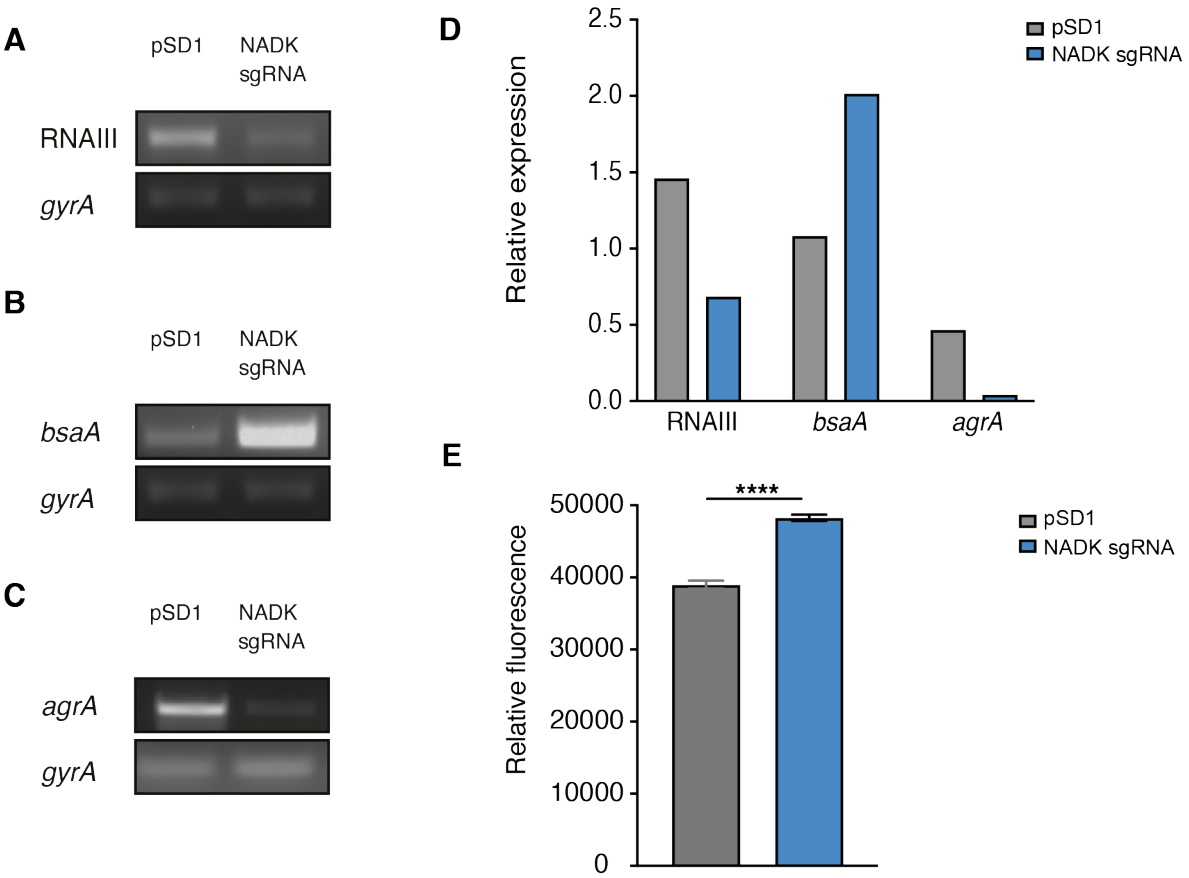

Figure 5 NADK is required for AgrA expression and *S. aureus* redox control. The *S. aureus* strain containing the empty vector (pSD1) and the *ppnK* knockdown strain (NADK sgRNA) were grown aerobically in BHI broth at 37°C for 4 hours. (A-C) RNA was extracted and subjected to RT-PCR using oligonucleotides specific to *gyrA*, RNAIII, *bsaA* and *agrA* genes, respectively. (D) Relative gene expression was normalized to *gyrA* transcript levels. (E) *S. aureus* ROS levels were quantified using the $DCFH_2$-DA assay. Comparison of data was performed using t-test (****$p<0.0001$). Data are representative of at least three independent experiments.

357 **Discussion**

358 The ability of *S. aureus* to survive and thrive in a wide variety of niches during infection,
359 ranging from skin to deeper tissues and abiotic devices, mirrors highly plastic metabolic
360 capacities allowing adaptive responses to constantly changing microenvironments (Potter et al.,
361 2020). Metabolic pathways are not only necessary for nutrient acquisition to sustain bacterial
362 growth, but also for regulation of virulence and are therefore central to host-pathogen
363 interactions (Eisenreich et al., 2010; Harper et al., 2018; Richardson, 2019; Teoh et al., 2021;
364 Tomlinson et al., 2021).

365 Here we show for the first time that NADK contributes to bacterial pathogenic potential.
366 NADK was necessary for successful *S. aureus* infection of zebrafish larvae, ultimately leading
367 to neutropenia and death. Decreasing NADK activity led to decreased host mortality without
368 affecting bacterial burden initially, suggesting that NADK promotes virulence factor activity
369 and/or counteracts host defenses independently of its contribution to bacterial growth capacity.
370 Besides neutrophils, macrophages are crucial cells in the innate immune defense against
371 infection. We uncovered that inhibition of *S. aureus* NADK activity has a major impact on
372 bacteria interactions with macrophages, reducing dramatically bacterial survival after
373 phagocytosis. We demonstrated that NADK contributes to resistance to ROS produced by
374 macrophages, neutralizing an important defense mechanism against bacterial infection (Pidwill
375 et al., 2021). Along the same lines, we showed that NADK protected *S. aureus* from hydrogen
376 peroxide toxicity. NADK, as the only source of NADP(H), is a key component of defense
377 against oxidative stress (Grose et al., 2006; Mailloux et al., 2011). In bacteria, it has been shown
378 that NADK activity is increased upon exposure to oxidative stress, acting as a metabolic switch
379 to decrease the NAD^+ pool which fuels ROS formation and increase the NADPH pool which
380 promotes ROS scavenging activities (Singh et al., 2007). Analysis of *S. aureus* proteome
381 revealed a drop in the levels of major antioxidant enzymes upon inhibition of *ppnK* expression.

382 By supporting superoxide dismutase, catalase, methionine sulfoxide reductase and other
383 antioxidant enzymes, NADK could prevent damages caused by ROS formed during
384 phagocytosis. However, antioxidant treatment of infected macrophages using NAC only
385 partially mitigated growth defect of the NADK knockdown strain. NADK might thus contribute
386 to bacterial survival within macrophages through pathways other than ROS detoxification. We
387 showed that inhibition of *ppnK* expression led to growth defect upon envelope stress, a
388 condition that is encountered in the host, particularly in macrophages where bacteria face
389 antimicrobial peptides and hydrolytic enzymes such as lysozyme (Rosenberger et al., 2004;
390 Cohn and Wiener, 1963; Callewaert and Michiels, 2010). *S. aureus* resists lysozyme through
391 peptidoglycan modification by the *O*-acetyltransferase OatA (Bera et al., 2005, 2006).
392 Regulation by the glycopeptide resistance-associated two-component system GraRS and D-
393 alanylation of teichoic acid by the *dlt* operon gene products also contribute to *S. aureus*
394 resistance to lysozyme, as well as CAMP (Herbert et al., 2007). OatA, DltA and GraRS were
395 less abundant when NADK was knocked down, suggesting that NADK could help *S. aureus*
396 resist antibacterial envelope-targeting compounds produced by macrophages and/or secreted
397 by the host. Strikingly, our proteomic analysis also highlighted the contribution of NADK to
398 production of virulence factors. Among them, PSM-alpha peptides have previously been shown
399 to lyse leucocytes, elicit phagosomal escape and play a key role in pathogenesis (Wang et al.,
400 2007; Kobayashi et al., 2011; Peschel and Otto, 2013; Grosz et al., 2014; Kitur et al., 2015).
401 The pore-forming toxin alpha-hemolysin has also been demonstrated to lyse leukocytes and is
402 required for full virulence in mouse, rabbit, and rat models of infection (Patel et al., 1987;
403 O'Callaghan et al., 1997; McElroy et al., 1999; Kitur et al., 2015; Seilie and Wardenburg,
404 2017). Gamma-hemolysin leucocidin is leukotoxic as well and contributes to *S. aureus*
405 bacteremia (Nilsson et al., 1999; Spaan et al., 2014). Control of these factors by NADK could
406 thus promote bacterial survival in macrophages and zebrafish, and trigger macrophage and

407 neutrophil death upon *S. aureus* infection. Remarkably, we found that inhibition of *ppnK*
408 expression decreases abundance of AgrA, the response regulator of *S. aureus agr* system at the
409 center of quorum-sensing and virulence. AgrA directly enhances the transcription of the PSM-
410 alpha genes and governs RNAIII-dependent expression of multiple virulence enzymes
411 including alpha-hemolysin and leukocidins (Queck et al., 2008). Thus, the contribution of
412 NADK to production of virulence factors is presumably mediated through AgrA. NADK
413 regulated expression of RNAIII and BsaA similarly to AgrA, corroborating this hypothesis.
414 Besides lowering abundance of AgrA, NADK knockdown led to decreased levels of *agrA*
415 transcript. Increased ROS levels detected in the knockdown strain could account for this
416 regulation as transcription of the *agr* operon is repressed in oxidative conditions (Rothfork et
417 al., 2004; Baker et al., 2010; Sun et al., 2012). Additionally, oxidation leads to formation of an
418 intramolecular disulfide bond between Cys-199 and Cys-228 in the DNA binding domain of
419 AgrA, thereby introducing a conformational change disrupting its association to promoter
420 region of target genes (Sun et al., 2012). A recent study confirmed oxidation sensing of the *agr*
421 system and revealed another mode of AgrA regulation by CoAlation of redox-active Cys199
422 inhibiting its DNA-binding activity (Bakovic et al., 2021).
423 In summary, our study shows that NADK supports production of protective enzymes,
424 virulence determinants and the response regulator AgrA, possibly by controlling the bacterial
425 redox state, ultimately promoting *S. aureus* pathogenic potential. NADK inhibition and quorum
426 quenching are attractive therapeutic approaches. Further investigations are now required to
427 fully understand the contribution of bacterial NADKs during infection processes and develop
428 chemical inhibitors that could be used in combination with current antibiotics to fight multidrug
429 resistant bacteria.
430

431 # Materials and methods

432 **Plasmids, bacterial strains, cell lines and culture conditions**

433 Bacterial strains and plasmids used in this study are listed in Table 3. All plasmids were
434 maintained in *Escherichia coli* TOP10. The restriction deficient *Staphylococcus aureus* strain
435 RN4220 was transformed with plasmids isolated from *E. coli*. The *S. aureus* Xen36 strain was
436 transformed with plasmids isolated from the RN4220 strain as previously described (Gelin et
437 al., 2020). *E. coli* was grown in lysogeny broth (LB) medium (Difco) with shaking at 200 rpm
438 or on LB agar plates at 37°C. *S. aureus* was grown in brain heart infusion (BHI) broth (BD) or
439 in tryptic soy broth (TSB) (Difco) with shaking at 200 rpm or on BHI agar plates at 37°C. When
440 required, culture medium was supplemented with antibiotics (carbenicillin 100 µg/mL for *E.*
441 *coli*, chloramphenicol 15 µg/mL or anhydrotetracycline 100 ng/mL for *S. aureus*). RAW 264.7
442 macrophages (TIB-71, ATCC) were cultured in DMEM (Gibco) containing 10 % FCS (Gibco).
443 Macrophages were seeded into 24-well plates at 10^5 cells per well.

444

445 **Table 3** Strains and plasmids used in this study.

Strain/plasmid	Relevant characteristics	Reference
Strains		
E. coli strain		
TOP10	F$^-$ *mcrA Δ(mrr-hsdRMS-mcrBC) ϕ80lacZ ΔM15 ΔlacX74 recA1 araD139 Δ(ara-leu) 7697 galU galK λ$^-$ rpsL*(Str^R) *endA1 nupG*	Invitrogen
S. aureus strains		
Xen36	Strain derived from a clinical isolate from a bacteremic patient	PerkinElmer, ATCC49525
Xen36/pSD1	Xen36 strain carrying plasmid pSD1	Gelin et al., 2020
Xen36/NADK sgRNA	Xen36 strain carrying plasmid pSD1 *ppnK*	Gelin et al., 2020
RN4220	Restriction-deficient strain derived from NCTC 8325-4	Kreiswirth et al., 1983
Plasmids		
pSD1	dCas9 ATc-inducible and sgRNA constitutive expression plasmid	Zhao et al., 2017
pSD1 *ppnK*	pSD1 plasmid carrying sgRNA targeting *S. aureus ppnK*	Gelin et al., 2020

446

447

448

449

450 **Table 4** Primers used in this study

Primer	Sequence (5'-3')
RT-ppnK-F	GTGACTCCAAGTCTAATGCC
RT-ppnK-R	ATTTTTCAACTTCATGAGGTAACC
RT-gyrA-F	GTGTTATCGTTGCTCGTG
RT-gyrA-R	CGGTGTCATACCTTGTTC
RT-RNAIII-F	AGTTTCCTTGGACTCAGTGCT
RT-RNAIII-R	AGGGGCTCACGACCATACTT
RT-bsaA-F	GCGAAGAAGCAGCTCAAAAC
RT-bsaA-R	CCTTCGCGATCCACTAAAAA
RT-agrA-F	GCCCTCGCAACTGATAATCC
RT-agrA-R	CACCGATGCATAGCAGTGTTC
RT-rluA-F	CCGCGAGAAATACCGAGTGT
RT-rluA-R	TCTCCCACAATTGGATGCCC
RT-operon-F1	TGACTTGCTTAAAAAGCACACTG
RT-operon-R1	ACGAGCATTTGTCCTACTTCAGA
RT-operon-F2	AACCGTTGAAGAAACATTCGACA
RT-operon-R2	GACGCTTGTTCACCAACTTCA
RT-operon-F3	CATCGTTTGGAAAGAGCGGC
RT-operon-R3	GGCATTAGACTTGGAGTCACCT
RT-operon-F4	ACGTGTGCACGATTCTTTCAT
RT-operon-R4	ATGGCGCTCACTGTCTTCT
RT-operon-F5	AGTTCATTTGCATACGGGACG
RT-operon-R5	ACGCTCTTTTTCATCTGTGTTCA
RT-operon-F6	TAACTTGTGCGATGACGGTGG
RT-operon-R6	TTCCAATCACAATCCCCATCAA
RT-operon-F7	ACGTTGATGAATTGAAGCAAGAG
RT-operon-R7	ACTTTAGCGACACCAAAAGCA
RT-operon-F8	TCAAGTGGCGTTACAGGTGA
RT-operon-R8	TTCAAATACCGCCAACGCAT

451

452 **Bacterial growth measurement**

453 *S. aureus* strains were grown overnight in BHI broth at 37°C and diluted to OD_{600nm}=0.05 into
454 BHI broth. For NADK inhibition experiments, culture medium was supplemented with 100
455 ng/mL anhydrotetracycline (Sigma-Aldrich) and 15 µg/mL chloramphenicol when required.
456 For stress experiments, culture medium was supplemented with hydrogen peroxide (0 to 500
457 µM), catalase (10 µg/mL), lysozyme (5 mg/mL) or lysostaphin (0.05 mg/mL). Bacterial
458 suspensions were incubated in 96-well plates with shaking at 200 rpm at 37°C. Growth was
459 monitored with a microplate reader (Glomax Discover, Promega). Experiments were performed
460 at least three times.

461

462

463

464 **Christie-Atkins-Munch-Peterson test**

465 *S. aureus* hemolytic activity was performed as described previously (Adhikari et al. 2007).
466 Briefly, *S. aureus* RN4220 was streaked vertically at the center of a sheep blood agar plate. *S.*
467 *aureus*/pSD1 and *S. aureus*/NADK sgRNA strains were then streaked perpendicularly to the
468 RN4220 strain. The plate was incubated at 37°C for 18 hours. Blood agar plates were then
469 photographed with a Scan500 imager (Interscience). The assay was repeated three times.

470

471 **RNA extraction and RT-PCR**

472 Bacteria grown for 4 h were collected by centrifugation 20 min at 15,000 x *g* at 4°C. Bacterial
473 lysis was performed using Precellys lysing kit (P000914-LYSK0-A) and the Precellys program
474 4 (6.500 rpm for 30 sec) twice at 4°C. RNA extraction was performed in 1 mL of TRIzol
475 (Invitrogen) according to the manufacturer's recommendations. RT-PCR was carried out with
476 Superscript one step RT kit (Invitrogen). Primers used are indicated in Table 4. RT-PCR assays
477 were repeated at least three times.

478

479 **Immunoblotting**

480 Bacteria grown for 4 h were collected by centrifugation 10 min at 10,000 x *g* at 4° C and
481 resuspended in 500 µL of PBS. Bacteria were lysed using the Precellys lysing kit (P000914-
482 LYSK0-A) and the Precellys program 4 (6,500 rpm for 30 sec) twice at 4°C. Lysates were
483 centrifuged for 15 min at 10,000 x *g* at 4 °C and supernatants were collected for protein
484 quantification using the Quick start Bradford protein assay kit 2 (Biorad). Samples were mixed
485 with Laemmli buffer (Biorad) and 10% β-mercaptoethanol and denatured for 5 min at 95°C.
486 Samples were separated onto 4−20% Miniprotean TGX stain-free precast gel (Biorad) in TGS
487 buffer and transferred on polyvinylidene fluoride membranes. Membranes were incubated
488 overnight at 4°C with primary antibodies diluted in 5% blotto (R114 rabbit anti-EF-Tu

489 polyclonal antibodies, 1:5000; R250 rabbit polyclonal anti-*S. aureus* NADK antibodies,
490 1:1000; anti-staphylococcal α-toxin (α-hemolysin) rabbit antiserum (Sigma-Aldrich S7531)
491 1:1000). Membranes were then incubated with 1:2500 antirabbit horseradish peroxidase-
492 conjugated antibodies (Abcam). Blots were revealed using the ECL kit (Pierce).
493
494 **RAW 264.7 macrophage infection**
495 RAW 264.7 macrophages were seeded into 24-well plates at 100,000 cells per well. *S. aureus*
496 Xen36/pSD1 and *S. aureus* Xen36/NADK sgRNA strains were grown to an OD_{600nm} of 0.6,
497 washed three times and diluted in DMEM to obtain a multiplicity of infection (MOI) of 10.
498 Infected macrophages were centrifugated at 500 x *g* for 5 min and incubated for 15 min at 37°C
499 and 5% CO_2 to synchronize phagocytosis. The medium was replaced with DMEM containing
500 gentamicin (20 µg/mL) for 30 min to kill extracellular bacteria. Cells were washed three times
501 in DPBS and incubated in DMEM supplemented with 100 ng/mL anhydrotetracycline and 10
502 mM N-acetyl cysteine (NAC, Sigma-Aldrich) when indicated. Cells were incubated for 6 h at
503 37°C and 5% CO_2. At each time points, cells were lysed in 0.2% Triton X-100 for 10 min at
504 37°C. The number of bacteria released from the cells was determined by plating serial dilutions
505 of the lysates on BHI agar plates that were incubated at 37°C for colony-forming units (CFU)
506 enumeration.
507
508 **Immunofluorescence assay**
509 RAW 264.7 macrophages were cultured on glass coverslips in 24-well plates. At 6 h post-
510 infection, cells were fixed in paraformaldehyde (PFA) 4% for 15 min, permeabilized for 4 min
511 with 0.1% Triton X-100 in 1% bovine serum albumin (BSA)-PBS and blocked in 1% BSA-
512 PBS. Fixed cells were incubated for 30 min with rabbit anti-*S. aureus* (Abcam ab20920) and
513 rat anti-LAMP1 1D4B (Abcam ab25245) primary antibodies. Cells were then incubated for 30
514 min with goat anti-rabbit Cy5 (Immunoresearch 111 175 144) or goat anti-rat FITC (Invitrogen

515 A11006) secondary antibodies and DAPI (10 µg/mL). Slides were mounted with Fluoromount
516 G (Invitrogen). Samples were observed with a Zeiss Axiovert 200M epifluorescence
517 microscope equipped with a Plan-apochromat objective (100X/1.4 Oil Ph3; Carl Zeiss, Inc.).
518 Images were acquired with a CCD camera Coolsnap, processed with Metamorph software v.6
519 (Molecular Devices) and analyzed with ImageJ software.
520

521 **Cytotoxicity assay**

522 Overnight cultures of *S. aureus*/pSD1 and *S. aureus*/NADK sgRNA were diluted to an OD_{600nm}
523 0.05 in BHI supplemented with ATc (100 ng/mL) and chloramphenicol (7 µg/mL), spread in a
524 96 wells plate and incubated for 6 hours at 37°C with shaking at 200 rpm. After 5h30 of growth,
525 lysozyme (5 mg/mL) and lysostaphin (0.05 mg/mL) were added. At t=6h, 100 µL of the CellTox
526 Green Reagent (1:500, G8741, Promega) were added to bacteria. After incubation at RT for 15
527 min, both OD_{600nm} and fluorescent signal (excitation at 475 nm, emission at 500-550 nm) were
528 measured with a microplate reader (Glomax Discover, Promega).
529 For the cytotoxicity assay on infected macrophages, culture medium was replaced by either
530 DPBS or by 0.2% Triton X-100 6 hours after the infection. After 10 min at 37°C, cells were
531 washed with DPBS, and then incubated with 100 µL of CellTox Green Reagent for 15 min at
532 RT. Fluorescent signal (excitation at 475 nm, emission at 500-550 nm) was measured with a
533 microplate reader (Glomax Discover, Promega).
534

535 **ROS levels quantification**

536 Overnight cultures of *S. aureus*/pSD1 and *S. aureus*/NADK sgRNA were diluted to an OD_{600nm}
537 0.05 in BHI supplemented with with ATc (100 ng/mL) and chloramphenicol (7 µg/mL), spread
538 in a 24 wells plate and incubated at 37°C with shaking at 200 rpm for 4h. After 4h, the OD_{600nm}
539 was measured and adjusted to 1, then bacteria centrifugated for 3 min at 13.000g. $DCFH_2$-DA

540 (5 mM) was mixed with NaOH (0.1 M) to obtain DCF. Bacterial pellets were resuspended in
541 100 uL of DCF and incubated for 40 min at RT protected from light in a 96-wells black plate.
542 Then fluorescence signal (excitation 475 nm, emission 500-550 nm) was measured with a
543 microplate reader (Glomax Discover, Promega).
544
545 **Ethics Statement**
546 Animal experiments were performed according to European Union guidelines for handling of
547 laboratory animals (http://ec.europa.eu/environment/chemicals/lab_animals/home_en.htm).
548 All experiments performed on larvae older than 5 days post fertilization were approved by the
549 Institut Pasteur Animal Care and Use Committee and the French Ministry of Education,
550 Research and Innovation, and registered under the reference APAFIS#31827.
551
552 **Zebrafish care and maintenance**
553 Homozygous Tg*(mfap4::mCherryF)* (ump6Tg) (Phan et al., 2018) Tg(*mpx::GFP*)^{i114}
554 (Renshaw et al., 2006) double transgenic fishes were raised in our facility. Eggs were obtained
555 by natural spawning, bleached according to standard protocols, and then kept in Petri dishes
556 containing Volvic spring water and, from 24 h hpf onwards, 0.003% 1-phenyl-2-thiourea (PTU)
557 (Sigma-Aldrich) was added to prevent pigmentation. Embryos were reared at 28°C or 24°C
558 according to the desired speed of development; infected larvae were always kept at 28°C. All
559 timings in the text refer to the developmental stage at the reference temperature of 28°C. Larvae
560 were anesthetized with 200 µg/ml of buffered tricaine methane sulfonate (MS-222, Sigma-
561 Aldrich) during the injection procedure as well as during *in vivo* imaging and processing for
562 bacterial burden evaluation.
563
564

565 **Zebrafish infection**

566 The volume of injected bacterial suspension was deduced from the diameter of the drop
567 obtained after mock microinjection, as previously described (Levraud et al., 2008). Bacteria
568 were diluted from overnight cultures and allowed to reach exponential growth. Then, they were
569 recovered by centrifugation, washed, and resuspended at the desired concentration in PBS. 55-
570 60 hours post-fertilization, anesthetized zebrafish larvae were microinjected intravenously (IV)
571 with 1 nL of bacterial suspension at the desired dose as described (Colucci-Guyon et al., 2011;
572 Mostowy et al., 2013). Infected larvae were transferred into individual wells containing 1 mL
573 of Volvic water and 0.003% PTU in 24-well culture plates, incubated at 28°C and regularly
574 observed under a stereomicroscope.

575

576 **Evaluation of the bacterial burden in infected zebrafish larvae**

577 Infected zebrafish larvae were collected at 0, 24, 48 and 72 hpi and lysed for the evaluation of
578 the bacterial burden as previously described (Boucontet et al., 2018; Mostowy et al., 2013).
579 Each larva was placed in an individual 1.5 mL Eppendorf tube and anesthetized with tricaine
580 (200 µg/mL), washed with 1 mL of sterile water, and placed in 150 µL of sterile water. Larvae
581 were then homogenized using a pestle motor mixer (Argos). Each sample was transferred to an
582 individual well of a 96-well plate and 10 X serial dilutions were performed. For CFU
583 enumeration and to assess plasmid stability throughout the infection kinetics, serial dilutions of
584 lysates were plated on BHI agar plates with and without chloramphenicol (15 µg/mL), that were
585 incubated overnight at 37°C.

586

587 **Zebrafish live imaging, image processing and analysis**

588 Quantification of total macrophages and neutrophils on living transgenic reporter larvae was
589 performed upon infection as we previously described (Mostowy et al., 2013). Briefly, bright

590 field, GFP and RFP images of whole living anesthetized larvae were taken using a Leica
591 Macrofluo™ Z16 APOA (zoom 16:1) macroscope equipped with a Leica PlanApo 2.0X lens,
592 and a Photometrics® CoolSNAP™ *HQ2* camera. Images were captured using the Metavue
593 software version 7.5.6.0 (MDS Analytical Technologies). After capture of images, larvae were
594 washed and transferred in a new 24-well plate filled with 1 mL of fresh water per well and
595 incubated at 28°C.
596
597 **Whole-mount immunohistochemistry and confocal imaging**
598 Whole larvae were fixed in 4% formaldehyde/PBS overnight at 4°C. After washes in PBSDT
599 (PBS, 1% DMSO, and 0.1% Tween), fixed larvae were treated with acetone at -20° for 20 min,
600 rinsed with 1× HBSS/0.1% Tween, permeabilized with a collagenase solution for up to 1 h
601 (Svoboda et al., 2001), washed in PBSDT, blocked with 10% Western Blocking Reagent
602 (Merck; 11921673001)/PBSDT, and then incubated for 24-48 h at 4°C with the primary
603 antibodies. Chicken anti-GFP (1:1000, ab13970, Abcam), and anti-*Staphylococcus aureus*
604 (1:500, ab20920, Abcam) antibodies were used. Following washes, samples were blocked in
605 10% Western blocking solution/PBSDT before overnight incubation with secondary antibodies
606 at 4°C with agitation. The secondary antibodies were Alexa Fluor 488-conjugated goat anti-
607 chicken (1:1000, A11039, Invitrogen) and Cy™5-conjugated goat anti-rabbit (1:200, 111-175-
608 144, Jackson Immunoresearch). Larvae were progressively embedded in glycerol (for
609 conservation and microscopic observation) and mounted in lateral position for imaging.
610 Confocal fluorescent imaging of fixed injected larvae was performed as previously described
611 (Colucci-Guyon et al., 2020). Briefly, injected larvae were positioned in lateral position in 35
612 mm glass-bottom µ-Dishes (81158, Ibidi). Larvae were immobilized in the dish using a drop of
613 1% low-melting-point agarose (V2111, Promega) solution in 80% glycerol. A Leica SP8
614 confocal microscope equipped with two PMT and one Hybrid detector, a 20X multi-IMM

615 (water-oil-glycerol) objective (HC PL APO CS2 20X/0.75), a X–Y motorized stage and the
616 LAS-X software were used to image injected larvae. All samples were acquired using the same
617 settings.
618
619 **Total protein extraction**
620 For *in vitro* samples, overnight cultures of *S. aureus*/pSD1 and *S. aureus*/NADK sgRNA were
621 diluted to an OD_{600nm} 0.05 in BHI with 200 µM H_2O_2 when indicated, spread in a 24-well plate
622 and incubated at 37°C with shaking at 200 rpm. After 6 h, bacteria were centrifugated for 15
623 min at 10,000 *g* at 4°C and the bacterial pellets were stored at -80°C. For *in vivo* samples,
624 zebrafish larvae were infected with *S. aureus*/pSD1 or *S. aureus*/NADK sgRNA strains (see
625 above). At 12 hpi, 5 larvae of each condition were isolated, anesthetized with tricaine, washed
626 with 1 mL of sterile water, dried, placed on dry ice and stored at -80°C. All samples were then
627 resuspended in 1 mL of Tris 100 mM pH 7/urea 8M. Proteins were extracted using the Precellys
628 kit SK38 (P000915-LYSK0-A0, Bertin), in a Cryolys homogenizer (Bertin) by 6 cycles of
629 agitation at 6,500 rpm for 15 s and 30 s rest.
630
631 **Protein digestion and cleanup of peptides**
632 Proteins were reduced using 5mM TCEP for 30 min at room temperature. Alkylation of the
633 reduced disulfide bridges was performed using 10mM iodoacetamide for 30 min at room
634 temperature in the dark. Proteins were then digested in two steps, first with 1 µg r-LysC Mass
635 Spec Grade (Promega) for 4 h at 30°C and then samples were diluted below 2 M urea with 100
636 mM Tris HCl pH 8.5 and 1 µg Sequencing Grade Modified Trypsin was added for the second
637 digestion overnight at 37°C. Proteolysis was stopped by adding formic acid (FA) at a final
638 concentration of 5%. The peptide samples were cleaned using C_{18} cartridges (Agilent
639 Technologies) in the automated AssayMAP Bravo Platform. The protocol for peptide cleanup

640 included in the platform was used as scaffold using the following settings. Cartridges were
641 primed with 100 µL of 100% acetonitrile (ACN) at 300 µL/min. Equilibration was done with
642 50 µL of 0.1% FA at 10 µL/min. The sample was loaded at 5 µL/min. Cup wash (25 µL) and
643 the internal cartridge wash (50 µL at 10 µL/min) were performed with 0.1% FA. Peptides were
644 eluted with 50 µL of 50% ACN/0.1% FA at 5 µL/min. Samples were dried and stored at −80
645 °C until further use. Peptides were resuspended in 2% acetonitrile (ACN)/0.1% FA prior to LC-
646 MS injection.
647
648 **Liquid chromatography-mass spectrometry**
649 LC-MS/MS analysis was performed on a Orbitrap Q Exactive™ Plus Mass Spectrometer
650 (Thermo Fisher Scientific) coupled with a Proxeon EASY-nLC 1200 (Thermo Fisher
651 Scientific). One µg of peptides was injected onto a home-made 30 cm C_{18} column (1.9 µm
652 particles, 100 Å pore size, ReproSil-Pur Basic C18, Dr. Maisch GmbH, Ammerbuch-Entringen,
653 Germany). Column equilibration and peptide loading were done at 900 bars in buffer A (0.1%
654 FA). Peptides were separated with a multi-step gradient from 2 to 7 % buffer B (80% ACN,
655 0.1% FA) in 5 min, 7 to 23 % buffer B in 70 min, 23 to 45 % buffer B in 30 min at a flow rate
656 of 250 nL/min. Column temperature was set to 60°C. MS data were acquired using Xcalibur
657 software using a data-dependent method. MS scans were acquired at a resolution of 70,000 and
658 MS/MS scans (fixed first mass 100 m/z) at a resolution of 17,500. The AGC target and
659 maximum injection time for the survey scans and the MS/MS scans were set to $3E^6$, 20ms and
660 $1E^6$, 60ms respectively. An automatic selection of the 10 most intense precursor ions was
661 activated (Top 10) with a 45 s dynamic exclusion. The isolation window was set to 1.6 m/z and
662 normalized collision energy fixed to 28 for HCD fragmentation. We used an underfill ratio of
663 1.0 % corresponding to an intensity threshold of $1.7E^5$. Unassigned precursor ion charge states
664 as well as 1, 7, 8 and >8 charged states were rejected and peptide match was disabled.

665

666 **Data analysis**

667 Acquired Raw files were analyzed using the MaxQuant software version 1.6.6.0 (Cox et al.,
668 2011) using the Andromeda search engine (Cox and Mann, 2008; Tyanova et al., 2016). Sample
669 were grouped by type of experiment. The MS/MS spectra were searched against the
670 Staphylococcus aureus Uniprot reference proteome (2,889 entries).

671 All searches were performed with oxidation of methionine and protein N-terminal
672 acetylation as variable modifications and cysteine carbamidomethylation as fixed modification.
673 Trypsin was selected as protease allowing for up to two missed cleavages. The minimum
674 peptide length was set to 5 amino acids and the peptide mass was limited to a maximum of
675 8,000 Da. The false discovery rate (FDR) for peptide and protein identification was set to 0.01.
676 The main search peptide tolerance was set to 4.5 ppm and to 20 ppm for the MS/MS match
677 tolerance. Second peptides were enabled to identify co-fragmentation events. One unique
678 peptide to the protein group was required for the protein identification. A false discovery rate
679 cut-off of 1 % was applied at the peptide and protein levels. The mass spectrometry proteomics
680 data have been deposited to the ProteomeXchange Consortium via the PRIDE partner
681 repository with the dataset identifier PXD032968.

682 The statistical analysis of the proteomics data was performed as follows: Five biological
683 replicates were acquired per condition. To highlight significantly differentially abundant
684 proteins between two conditions, differential analyses were conducted through the following
685 data analysis pipeline: (1) deleting the reverse and potential contaminant proteins; (2) keeping
686 only proteins with at least three quantified values in one of the two compared conditions to limit
687 misidentifications and ensure a minimum of replicability; (3) log2-transformation of the
688 remaining intensities of proteins; (4) normalizing the intensities by median centering within
689 conditions thanks to the *normalizeD* function of the R package DAPAR (Wieczorek et al.,

690 2017), (5) putting aside proteins without any value in one of both compared conditions: as they
691 are quantitatively present in a condition and absent in another, they are considered as
692 differentially abundant proteins and (6) performing statistical differential analysis on them by
693 requiring a minimum fold-change of 2.5 between conditions and by using a LIMMA t test
694 (Smyth, 2005 ; Ritchie et al., 2015) combined with an adaptive Benjamini-Hochberg correction
695 of the p values thanks to the *adjust.p* function of the R package cp4p (Giai Gianetto et al., 2016).
696 The robust method of Pounds and Cheng was used to estimate the proportion of true null
697 hypotheses among the set of statistical tests (Pounds and Cheng, 2006). The proteins associated
698 with an adjusted p value inferior to an FDR level of 1% have been considered as significantly
699 differentially abundant proteins. Finally, the proteins of interest are therefore the proteins that
700 emerge from this statistical analysis supplemented by those being quantitatively absent from
701 one condition and present in another.
702
703 **Statistical analysis**
704 Results are expressed as means ± SEM of at least 3 replicates. Statistical analysis was performed
705 using GraphPad Prism (GraphPad Prism® 9.1.2. Software). One-way, two-ways ANOVA or t-
706 test were used to compare data. Differences between groups were considered significant when
707 the *p* value was lower than 0.05. Survival data were plotted using the Kaplan-Meier estimator
708 and log-rank (Mantel-Cox) tests were performed to assess differences between groups.
709
710

Aknowlegments

Authors are deeply indebted to Liliane Assairi, Sylvie Pochet and Gilles Labesse who led us into the world of NAD kinases. We are grateful to past and present members of the NADK consortium, all members of the *Yersinia* research unit and the French national reference center for plague and other yersiniosis, as well as Frédéric Barras and Daniel Ladant for helpful discussions and insightful comments. We thank Changlong Zhao for providing pSD1. We also wish to thank the members of the fish facility team Yohann Rolin and Noël Aimar for their excellent care of the fish.

This work was funded by the Agence Nationale de la Recherche (grant ANR-17-CE18-0011-02) and supported by Institut Pasteur, Université Paris Cité and CNRS. The *Yersinia* Research Unit is member of the Laboratory of Excellence Integrative Biology of Emerging Infectious Diseases (ANR-10-LBX-62-IBEID). We are grateful for support for equipment from the French government Programme d'investissements d'avenir France BioImaging (ANR-10-INSB-04-01).

Competing interests

The authors declare no conflict of interest.

729 **References**

730

731 Adhikari RP, Arvidson S, Novick RP. 2007. A nonsense mutation in *agrA* accounts for the
732 defect in *agr* expression and the avirulence of *Staphylococcus aureus* 8325-4 traP::kan.
733 *Infect Immun* **75**:4534-40. doi: 10.1128/IAI.00679-07.

734 Avican K, Aldahdooh J, Togninalli M, Mahmud AKMF, Tang J, Borgwardt KM, Rhen M,
735 Fällman M. 2021. RNA atlas of human bacterial pathogens uncovers stress dynamics linked
736 to infection. *Nat Commun* **12**:3282. doi:10.1038/S41467-021-23588-W

737 Baker J, Sitthisak S, Sengupta M, Johnson M, Jayaswal RK, Morrissey JA. 2010. Copper stress
738 induces a global stress response in *Staphylococcus aureus* and represses *sae* and *agr*
739 expression and biofilm formation. *Appl Environ Microbiol* **76**:150-160. doi:
740 10.1128/AEM.02268-09.

741 Baković J, Yu BYK, Silva D, Baczynska M, Peak-Chew SY, Switzer A, Burchell L,
742 Wigneshweraraj S, Vandanashree M, Gopal B, Filonenko V, Skehel M, Gout I. 2021. Redox
743 regulation of the quorum-sensing transcription factor AgrA by coenzyme A. *Antioxidants*
744 **10**:841. doi: 10.3390/antiox10060841

745 Bera A, Biswas R, Herbert S, Götz F. 2006. The presence of peptidoglycan *O*-acetyltransferase
746 in various staphylococcal species correlates with lysozyme resistance and pathogenicity.
747 *Infect Imm* **74**: 4598-4604. doi:10.1128/IAI.00301-06

748 Bera A, Herbert S, Jakob A, Vollmer W, Götz F. 2005. Why are pathogenic staphylococci so
749 lysozyme resistant? The peptidoglycan O-acetyltransferase OatA is the major determinant
750 for lysozyme resistance of *Staphylococcus aureus*. *Mol Microbiol* **55**:778-87. doi:
751 10.1111/j.1365-2958.2004.04446.x

752 Berrin JG, Pierrugues O, Brutesco C, Alonso B, Montillet JL, Roby D, Kazmaier M. 2005.
753 Stress induces the expression of AtNADK-1, a gene encoding a NAD(H) kinase in

754 *Arabidopsis thaliana*. *Mol Genet Genomics* **273**:10–19. doi:10.1007/s00438-005-1113-1
755 Boucontet L, Passoni G, Thiry V, Maggi L, Herbomel P, Levraud J-P, Colucci-Guyon E. 2018.
756 A model of superinfection of virus-infected zebrafish larvae: increased susceptibility to
757 bacteria associated with neutrophil death. *Front Immunol* **9**:1084.
758 doi:10.3389/FIMMU.2018.01084
759 Callewaert L, Michiels CW. 2010. Lysozymes in the animal kingdom. *J Biosci.* **35**:127-160.
760 doi10.1007/s12038-010-0015-5
761 Chai M-F, Wei P-C, Chen Q-J, An R, Chen J, Yang S, Wang X-C. 2006. NADK3, a novel
762 cytoplasmic source of NADPH, is required under conditions of oxidative stress and
763 modulates abscisic acid responses in *Arabidopsis*. *Plant J* **47**:665–674. doi:10.1111/j.1365-
764 313X.2006.02816.x
765 Chandel NS. 2021. Carbohydrate metabolism. *Cold Spring Harb Perspect Biol* **13**:1–15.
766 doi:10.1101/CSHPERSPECT.A040568
767 Chaudhuri RR, Allen AG, Owen PJ, Shalom G, Stone K, Harrison M, Burgis TA, Lockyer M,
768 Garcia-Lara J, Foster SJ, Pleasance SJ, Peters SE, Maskell DJ, Charles IG. 2009.
769 Comprehensive identification of essential *Staphylococcus aureus* genes using Transposon-
770 Mediated Differential Hybridisation (TMDH). *BMC Genomics* **10**:291. doi:10.1186/1471-
771 2164-10-291
772 Chini CCS, Zeidler JD, Kashyap S, Warner G, Chini EN. 2021. Evolving concepts in NAD^+
773 metabolism. *Cell Metab*. **33**:1076-1087. doi:10.1016/j.cmet.2021.04.003
774 Cisani G, Varaldo PE, Grazi G, Soro O. 1982. High-level potentiation of lysostaphin anti-
775 staphylococcal activity by lysozyme. *Antimicrob Agents Chemother* **21**:531-535. doi:
776 10.1128/AAC.21.4.531.

777 Cohn ZA, Wiener E. 1963. The particulate hydrolases of macrophages. II. Biochemical and
778 morphological response to particle ingestion. *J Exp Med* **118**:1009-20. doi:
779 10.1084/jem.118.6.1009
780 Colucci-Guyon E, Rifflet A, Saint-Auret S, da Costa A, Boucontet L, Laval T, Prehaud C,
781 Blanchard N, Levraud JP, Boneca IG, Demangel C, Guenin-Macé L. 2020. Spatiotemporal
782 analysis of mycolactone distribution in vivo reveals partial diffusion in the central nervous
783 system. *PLoS Negl Trop Dis*. **14**:e0008878. doi: 10.1371/journal.pntd.0008878
784 Colucci-Guyon E, Tinevez J-Y, Renshaw SA, Herbomel P. 2011. Strategies of professional
785 phagocytes in vivo: unlike macrophages, neutrophils engulf only surface-associated
786 microbes. *J Cell Sci* **124**:3053–3059. doi:10.1242/JCS.082792
787 Covarrubias AJ, Perrone R, Grozio A, Verdin E. 2021. NAD^+ metabolism and its roles in
788 cellular processes during ageing. *Nat Rev Mol Cell Biol*. **22**:119–141. doi:10.1038/s41580-
789 020-00313-x
790 Cox J, Mann M. 2008. MaxQuant enables highpeptide identification rates, individualized
791 p.p.b.-range mass accuracies and proteome-wide protein quantification. *Nat Biotechnol*
792 **26**:1367–1372.
793 Cox J, Neuhauser N, Michalski A, Scheltema RA, Olsen JV, Mann M. 2011. Andromeda: A
794 peptide search engine integrated into the MaxQuant environment. *J Proteome Res* **10**:1794-
795 1805.
796 Eisenreich W, Dandekar T, Heesemann J, Goebel W. 2010. Carbon metabolism of intracellular
797 bacterial pathogens and possible links to virulence. *Nat Rev Microbiol* **8**:401–412.
798 doi:10.1038/NRMICRO2351
799 Fang FC. 2004. Antimicrobial reactive oxygen and nitrogen species: concepts and
800 controversies. *Nat Rev Microbiol* **2**:820-832. doi:10.1038/nrmicro1004
801 Fang FC, Frawley ER, Tapscott T, Vázquez-Torres A. 2016. Bacterial stress responses during

802 host infection. *Cell Host Microbe* **20**:133–143. doi:10.1016/J.CHOM.2016.07.009

803 Fisher DJ, Fernandez RE, Maurelli AT. 2013. *Chlamydia trachomatis* transports NAD via the
804 Npt1 ATP/ADP translocase. *J Bacteriol* **195**:3381-3386. doi:10.1128/JB.00433-13

805 Galione A, Chuang K-T. 2020. Pyridine nucleotide metabolites and calcium release from
806 intracellular stores. *Adv Exp Med Biol* **1131**:371–394. doi:10.1007/978-3-030-12457-1_15

807 Gelin M, Paoletti J, Huteau V, Nahori M, Leseigneur C, Dugue L, Clement D, Pons J, Assairi
808 L, Pochet S, Labesse G, Dussurget O. 2020. From substrate to fragments to inhibitor active
809 in vivo against *Staphylococcus aureus*. *ACS Infect Dis* **6**:422–435.
810 doi:10.1021/acsinfecdis.9b00368

811 Giai Gianetto Q, Combes F, Ramus C, Bruley C, Coute Y, Burger T. 2016. Calibration plot for
812 proteomics: a graphical tool to visually check the assumptions underlying FDR control in
813 quantitative experiments. *Proteomics* **16**: 29–32.

814 Grose H, Joss L, Velick SF, Roth JR. 2006. Evidence that feedback inhibition of NAD kinase
815 controls responses to oxidative stress. *Proc Natl Acad Sci USA* **103**:7601–7606.
816 doi:10.1073/pnas.0602494103

817 Grosz M, Kolter J, Paprotka K, Winkler AC, Schäfer D, Chatterjee SS, Geiger T, Wolz C,
818 Ohlsen K, Otto M, Rudel T, Sinha B, Fraunholz M. 2014. Cytoplasmic replication of
819 *Staphylococcus aureus* upon phagosomal escape triggered by phenol-soluble modulin alpha.
820 *Cell Microbiol* **16**:451-65. doi: 10.1111/cmi.12233

821 Harper L, Balasubramanian D, Ohneck EA, Sause WE, Chapman J, Mejia-Sosa B, Lhakhang
822 T, Heguy A, Tsirigos A, Ueberheide B, Boyd JM, Lun DS, Torres VJ. 2018. *Staphylococcus*
823 *aureus* responds to the central metabolite pyruvate to regulate virulence. *mBio* **9**:2272–2289.
824 doi:10.1128/mBio.02272-17

825 Herbert S, Bera A, Nerz C, Kraus D, Peschel A, Goerke C, Meehl M, Cheung A, Götz F. 2007.
826 Molecular basis of resistance to muramidase and cationic antimicrobial peptide activity of

827 lysozyme in staphylococci. *PLoS Pathog* **3**:e102. doi:10.1371/journal.ppat.0030102
828 Kawai S, Mori S, Mukai T, Suzuki S, Yamada T, Hashimoto W, Murata K. 2000. Inorganic
829 polyphosphate/ATP-NAD kinase of *Micrococcus flavus* and *Mycobacterium tuberculosis*
830 H37Rv. *Biochem Biophys Res Commun* **276**:57–63. doi:10.1006/bbrc.2000.3433
831 Kitur K, Parker D, Nieto P, Ahn DS, Cohen TS, Chung S, Wachtel S, Bueno S, Prince A. 2015.
832 Toxin-induced necroptosis is a major mechanism of *Staphylococcus aureus* lung damage.
833 *PLoS Pathog*. **11**:e1004820. doi: 10.1371/journal.ppat.1004820.
834 Kobayashi K, Ehrlich SD, Albertini A, Amati G, Andersen KK, Arnaud M, Asai K, Ashikaga
835 S, Aymerich S, Bessieres P, Boland F, Brignell SC, Bron S, Bunai K, Chapuis J, Christiansen
836 LC, Danchin A, Débarbouillé M, Dervyn E, Deuerling E, Devine K, Devine SK, Dreesen O,
837 Errington J, Fillinger S, Foster SJ, Fujita Y, Galizzi A, Gardan R, Eschevins C, Fukushima
838 T, Haga K, Harwood CR, Hecker M, Hosoya D, Hullo MF, Kakeshita H, Karamata D,
839 Kasahara Y, Kawamura F, Koga K, Koski P, Kuwana R, Imamura D, Ishimaru M, Ishikawa
840 S, Ishio I, le Coq D, Masson A, Mauël C, Meima R, Mellado RP, Moir A, Moriya S,
841 Nagakawa E, Nanamiya H, Nakai S, Nygaard P, Ogura M, Ohanan T, O'Reilly M, O'Rourke
842 M, Pragai Z, Pooley HM, Rapoport G, Rawlins JP, Rivas LA, Rivolta C, Sadaie A, Sadaie
843 Y, Sarvas M, Sato T, Saxild HH, Scanlan E, Schumann W, Seegers JFML, Sekiguchi J,
844 Sekowska A, Séror SJ, Simon M, Stragier P, Studer R, Takamatsu H, Tanaka T, Takeuchi
845 M, Thomaides HB, Vagner V, van Dijl JM, Watabe K, Wipat A, Yamamoto H, Yamamoto
846 M, Yamamoto Y, Yamane K, Yata K, Yoshida K, Yoshikawa H, Zuber U, Ogasawara N.
847 2003. Essential *Bacillus subtilis* genes. *Proc Natl Acad Sci USA* **100**:4678–4683.
848 doi:10.1073/pnas.0730515100
849 Kobayashi SD, Malachowa N, Whitney AR, Braughton KR, Gardner DJ, Long D, Bubeck
850 Wardenburg J, Schneewind O, Otto M, Deleo FR. 2011. Comparative analysis of USA300

851 virulence determinants in a rabbit model of skin and soft tissue infection. *J Infect Dis*
852 204:937-41. doi: 10.1093/infdis/jir441
853 Kornberg A. 1950. Enzymatic synthesis of triphosphopyrine nucleotide. *J Biol Chem* **182**:805–
854 813.
855 Kreiswirth BN, Löfdahl S, Betley MJ, O'Reilly M, Schlievert PM, Bergdoll MS, Novick RP.
856 1983. The toxic shock syndrome exotoxin structural gene is not detectably transmitted by a
857 prophage. *Nature* **305**:709–712. doi:10.1038/305709a0
858 Levraud J-P, Colucci-Guyon E, Redd MJ, Lutfalla G, Herbomel P. 2008. *In vivo* analysis of
859 zebrafish innate immunity. *Methods Mol Biol* **415**:337–363. doi:10.1007/978-1-59745-570-
860 1_20
861 Liebermeister W, Noor E, Flamholz A, Davidi D, Bernhardt J, Milo R. 2014. Visual account
862 of protein investment in cellular functions. *Proc Natl Acad Sci USA* **111**:8488-8493.
863 doi.org/10.1073/pnas.1314810111
864 Li B Bin, Wang X, Tai L, Ma TT, Shalmani A, Liu WT, Li WQ, Chen KM. 2018. NAD kinases:
865 Metabolic targets controlling redox co-enzymes and reducing power partitioning in plant
866 stress and development. *Front Plant Sci*. **9**:379. doi:10.3389/fpls.2018.00379
867 Li W, Wu H, Li M, San KY. 2018. Effect of NADPH availability on free fatty acid production
868 in *Escherichia coli*. *Biotechnol Bioeng* **115**:444–452. doi:10.1002/bit.26464
869 McElroy MC, Harty HR, Hosford GE, Boylan GM, Pittet JF, Foster TJ. 1999. Alpha-toxin
870 damages the air-blood barrier of the lung in a rat model of *Staphylococcus aureus*-induced
871 pneumonia. *Infect Immun* **67**:5541-4. doi: 10.1128/IAI.67.10.5541-5544.1999
872 Mailloux RJ, Lemire J, Appanna VD. 2011. Metabolic networks to combat oxidative stress in
873 *Pseudomonas fluorescens*. *Antonie van Leeuwenhoek* **99**:433–442. doi:10.1007/s10482-
874 010-9538-x
875 McGuinness ET, Butler JR. 1985. NAD^+ kinase - a review. *Int J Biochem* **17**:1–11.

876 Mostowy S, Boucontet L, Mazon Moya MJ, Sirianni A, Boudinot P, Hollinshead M, Cossart P,
877 Herbomel P, Levraud JP, Colucci-Guyon E. 2013. The zebrafish as a new model for the *in*
878 *vivo* study of *Shigella flexneri* interaction with phagocytes and bacterial autophagy. *PLoS*
879 *Pathog* **9**:12–16. doi:10.1371/journal.ppat.1003588
880 Nilsson IM, Hartford O, Foster T, Tarkowski A. 1999. Alpha-toxin and gamma-toxin jointly
881 promote *Staphylococcus aureus* virulence in murine septic arthritis. *Infect Immun.* **67**:1045-
882 9. doi: 10.1128/IAI.67.3.1045-1049.1999. PMID: 10024541; PMCID: PMC96427.
883 O'Callaghan RJ, Callegan MC, Moreau JM, Green LC, Foster TJ, Hartford OM, Engel LS, Hill
884 JM. 1997. Specific roles of alpha-toxin and beta-toxin during *Staphylococcus aureus* corneal
885 infection. *Infect Immun* **65**:1571-8. doi: 10.1128/iai.65.5.1571-1578.1997
886 Patel AH, Nowlan P, Weavers ED, Foster T. 1987. Virulence of protein A-deficient and alpha-
887 toxin-deficient mutants of *Staphylococcus aureus* isolated by allele replacement. *Infect*
888 *Immun* **55**:3103-10. doi: 10.1128/iai.55.12.3103-3110.1987
889 Peschel A, Otto M. 2013. Phenol-soluble modulins and staphylococcal infection. *Nat Rev*
890 *Microbiol* **11**:667-73. doi: 10.1038/nrmicro3110
891 Phan QT, Sipka T, Gonzalez C, Levraud J-P, Lutfalla G, Nguyen-Chi M. 2018. Neutrophils use
892 superoxide to control bacterial infection at a distance. *PLoS Pathog* **14**:e1007157.
893 doi:10.1371/JOURNAL.PPAT.1007157
894 Pidwill GR, Gibson JF, Cole J, Renshaw SA, Foster SJ. 2021. The role of macrophages in
895 *Staphylococcus aureus* infection. *Front Immunol* **11**:3506. doi:10.3389/fimmu.2020.620339
896 Pollitt EJG, Szkuta PT, Burns N, Foster SJ. 2018. *Staphylococcus aureus* infection dynamics.
897 *PLoS Pathog* **14**:e1007112. doi:10.1371/journal.ppat.1007112
898 Potter AD, Butrico CE, Ford CA, Curry JM, Trenary IA, Tummarakota SS, Hendrix AS, Young
899 JD, Cassat JE. 2020. Host nutrient milieu drives an essential role for aspartate biosynthesis
900 during invasive *Staphylococcus aureus* infection. *Proc Natl Acad Sci USA* **117**:12394–

901 12401. doi:10.1073/pnas.1922211117

902 Pounds S, Cheng C. 2006. Robust estimation of the false discovery rate. *Bioinformatics*
903 **22**:1979-87.

904 Prajsnar TK, Cunliffe VT, Foster SJ, Renshaw SA. 2008. A novel vertebrate model of
905 *Staphylococcus aureus* infection reveals phagocyte-dependent resistance of zebrafish to
906 non-host specialized pathogens. *Cell Microbiol* **10**:2312–2325. doi:10.1111/j.1462-
907 5822.2008.01213.x

908 Prajsnar TK, Hamilton R, Garcia‐Lara J, McVicker G, Williams A, Boots M, Foster SJ,
909 Renshaw SA. 2012. A privileged intraphagocyte niche is responsible for disseminated
910 infection of *Staphylococcus aureus* in a zebrafish model. *Cell Microbiol* **14**:1600–1619.
911 doi:10.1111/j.1462-5822.2012.01826.x

912 Queck SY, Jameson-Lee M, Villaruz AE, Bach TH, Khan BA, Sturdevant DE, Ricklefs SM,
913 Li M, Otto M. 2008. RNAIII-independent target gene control by the *agr* quorum-sensing
914 system: insight into the evolution of virulence regulation in *Staphylococcus aureus*. *Mol Cell*
915 **32**:150-8. doi: 10.1016/j.molcel.2008.08.005

916 Renshaw SA, Loynes CA, Trushell DMI, Elworthy S, Ingham PW, Whyte MKB. 2006. A
917 transgenic zebrafish model of neutrophilic inflammation. *Blood* **108**:3976–3978.
918 doi:10.1182/BLOOD-2006-05-024075

919 Richardson AR. 2019. Virulence and metabolism. *Microbiol Spectr* **7**.
920 doi:10.1128/microbiolspec.gpp3-0011-2018

921 Ritchie ME, Phipson B, Wu D, Hu Y, Law CW, Shi W, Smyth GK. 2015. Limma powers
922 differential expression analyses for RNA-sequencing and microarray studies. *Nucleic Acids*
923 *Res* **43**:e47. doi: 10.1093/nar/gkv007

924 Rosenberger CM, Gallo RL, Finlay BB. 2004. Interplay between antibacterial effectors: a
925 macrophage antimicrobial peptide impairs intracellular *Salmonella* replication. *Proc Natl*
926 *Acad Sci USA* **101**:2422-7. doi:10.1073/pnas.0304455101
927 Rothfork JM, Timmins GS, Harris MN, Chen X, Lusis A, Otto M, Cheung AL, Greshan HD.
928 2004. Inactivation of a bacterial virulence pheromone by phagocyte-derived oxidants: new
929 role for the NADPH oxidase in host defense. *Proc Natl Acad Sci USA* **101**:13867-72. doi:
930 10.1073/pnas.0402996101
931 Ruiz JM, Sánchez E, García PC, López-Lefebre LR, Rivero RM, Romero L. 2002. Proline
932 metabolism and NAD kinase activity in greenbean plants subjected to cold-shock.
933 *Phytochemistry* **59**:473–478. doi:10.1016/S0031-9422(01)00481-2
934 Sassetti CM, Boyd DH, Rubin EJ. 2003. Genes required for mycobacterial growth defined by
935 high density mutagenesis. *Mol Microbiol* **48**:77–84. doi:10.1046/j.1365-2958.2003.03425.x
936 Seilie ES, Bubeck Wardenburg J. 2017. *Staphylococcus aureus* pore-forming toxins: the
937 interface of pathogen and host complexity. *Semin Cell Dev Biol* **72**:101-116. doi:
938 10.1016/j.semcdb.2017.04.003
939 Singh R, Mailloux RJ, Puiseux-Dao S, Appanna VD. 2007. Oxidative stress evokes a metabolic
940 adaptation that favors increased NADPH synthesis and decreased NADH production in
941 *Pseudomonas fluorescens*. *J Bacteriol* **189**:6665–6675. doi:10.1128/JB.00555-07
942 Ślaski JJ. 1995. NAD^+ kinase activity in root tips of nearly isogenic linesof wheat (*Triticum*
943 *aestivum* L.) that differ in their tolerance to aluminium. *J Plant Physiol* **145**:143–147.
944 doi:10.1016/S0176-1617(11)81861-4
945 Smyth, GK. 2005. Limma: Linear models for microarray data. In: Gentleman, R., Carey, V.J.,
946 Huber, W., Irizarry, R.A., Dudoit, S. (eds) Bioinformatics and computational biology
947 solutions using R and bioconductor. Statistics for biology and health. Springer, New York,
948 NY. https://doi.org/10.1007/0-387-29362-0.23s

949 Spaan AN, Vrieling M, Wallet P, Badiou C, Reyes-Robles T, Ohneck EA, Benito Y, de Haas
950 CJ, Day CJ, Jennings MP, Lina G, Vandenesch F, van Kessel KP, Torres VJ, van Strijp JA,
951 Henry T. 2014. The staphylococcal toxins γ-haemolysin AB and CB differentially target
952 phagocytes by employing specific chemokine receptors. *Nat Commun* **5**:5438. doi:
953 10.1038/ncomms6438
954 Sun F, Liang H, Kong X, Xie S, Cho H, Deng X, Ji Q, Zhang H, Alvarez S, Hicks LM, Bae T,
955 Luo C, Jiang H, He C. 2012. Quorum-sensing *agr* mediates bacterial oxidation response via
956 an intramolecular disulfide redox switch in the response regulator AgrA. *Proc Natl Acad Sci*
957 *USA* **109**:9095-100. doi: 10.1073/pnas.1200603109
958 Svoboda KR, Linares AE, Ribera AB. 2001. Activity regulates programmed cell death of
959 zebrafish Rohon-Beard neurons. *Development* **128**:3511-20. doi: 10.1242/dev.128.18.3511
960 Tai L, Li B-B, Nie X-M, Zhang P-P, Hu C-H, Zhang L, Liu W-T, Li W-Q, Chen K-M. 2019.
961 Calmodulin is the fundamental regulator of NADK-mediated NAD signaling in plants. *Front*
962 *Plant Sci* **10**:681. doi:10.3389/fpls.2019.00681
963 Teoh WP, Chen X, Laczkovich I, Alonzo F 3rd. 2021. *Staphylococcus aureus* adapts to the host
964 nutritional landscape to overcome tissue-specific branched-chain fatty acid requirement.
965 *Proc Natl Acad Sci USA* **118**. doi:10.1073/PNAS.2022720118
966 Tomlinson KL, Lung TWF, Dach F, Annavajhala MK, Gabryszewski SJ, Groves RA, Drikic
967 M, Francoeur NJ, Sridhar SH, Smith ML, Khanal S, Britto CJ, Sebra R, Lewis I, Uhlemann
968 AC, Kahl BC, Prince AS, Riquelme SA. 2021. *Staphylococcus aureus* induces an itaconate-
969 dominated immunometabolic response that drives biofilm formation. *Nat Commun* **12**.
970 doi:10.1038/s41467-021-21718-y
971 Turner NA, Sharma-Kuinkel BK, Maskarinec SA, Eichenberger EM, Shah PP, Carugati M,
972 Holland TL, Fowler VG. 2019. Methicillin-resistant *Staphylococcus aureus*: an overview of
973 basic and clinical research. *Nat Rev Microbiol* **17**:203-218. doi:10.1038/s41579-018-0147-

974 4

975 Turner WL, Waller JC, Vanderbeld B, Snedden WA. 2004. Cloning and characterization of two
976 NAD kinases from *Arabidopsis*. Identification of a calmodulin binding isoform. *Plant*
977 *Physiol* **135**:1243–1255. doi:10.1104/pp.104.040428

978 Tyanova S, Temu T, Cox J. 2016. The MaxQuant computational platform for mass
979 spectrometry-based shotgun proteomics. *Nat Protoc* **11**:2301-2319.

980 Vestergaard M, Frees D, Ingmer H. 2019. Antibiotic resistance and the MRSA problem.
981 *Microbiol Spectr* **7**. doi:10.1128/microbiolspec.GPP3-0057-2018

982 Vestin R. 1937. Enzymic change from codehydrogenase I to codehydrogenase II.
983 *Naturwissenschaften* **25**:667–8.

984 Von Euler H, Adler E. 1938. Enzymic intertransformation of codehydrogenase I and
985 codehydrogenase II. *Z Physiol Chem* **252**:41–8.

986 Wang R, Braughton KR, Kretschmer D, Bach THL, Queck SY, Li M, Kennedy AD, Dorward
987 DW, Klebanoff SJ, Peschel A, DeLeo FR, Otto M. 2007. Identification of novel cytolytic
988 peptides as key virulence determinants for community-associated MRSA. *Nat Med* **13**:1501-
989 14. doi: 10.1038/nm1656

990 Wieczorek S, Combes F, Lazar C, Giai Gianetto Q, Gatto L, Dorffer A, Hesse AM, Couté Y,
991 Ferro M, Bruley C, Burger T. 2017. DAPAR & ProStaR: software to perform statistical
992 analyses in quantitative discovery proteomics. *Bioinformatics* **33**: 135-136.

993 Zhao C, Shu X, Sun B. 2017. Construction of a gene knockdown system based on catalytically
994 inactive ("dead") Cas9 (dCas9) in *Staphylococcus aureus*. *Appl Environ Microbiol* **83**.
995 doi:10.1128/AEM.00291-17

996

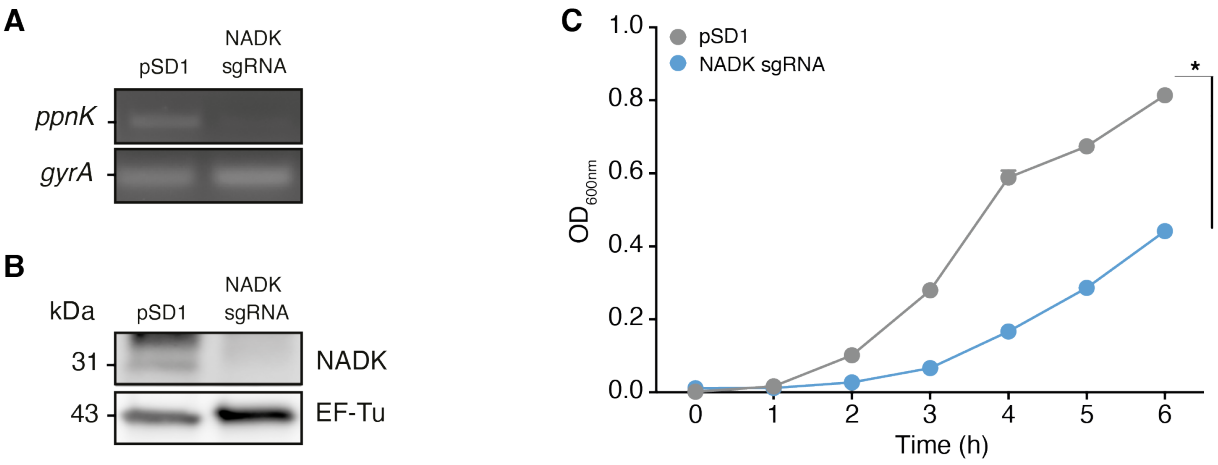

997

998 **Figure supplement 1** NADK is important for *S. aureus* growth. (A) Total RNAs of *S. aureus* containing the empty
999 vector (pSD1) or the NADK knockdown strain (NADK sgRNA) were analyzed by RT-PCR using oligonucleotides
1000 specific to the target gene *ppnK* or the control gene *gyrA*. (B) Bacterial protein extracts of *S. aureus* containing the
1001 empty vector (pSD1) or the NADK knockdown strain (NADK sgRNA) were analyzed by immunoblotting using
1002 antibodies against the target protein NADK or against the control protein EF-Tu. (C) Bacterial growth of *S. aureus*
1003 containing the empty vector (pSD1) or the NADK knockdown strain (NADK sgRNA) monitored for 6 hours at
1004 OD_{600nm} in BHI broth at 37°C upon ATc induction. Data shown are representative of three independent
1005 experiments. The bar indicates the standard error of the means of biological replicates. Comparison of data was
1006 performed using a t test (*$p<0.05$).

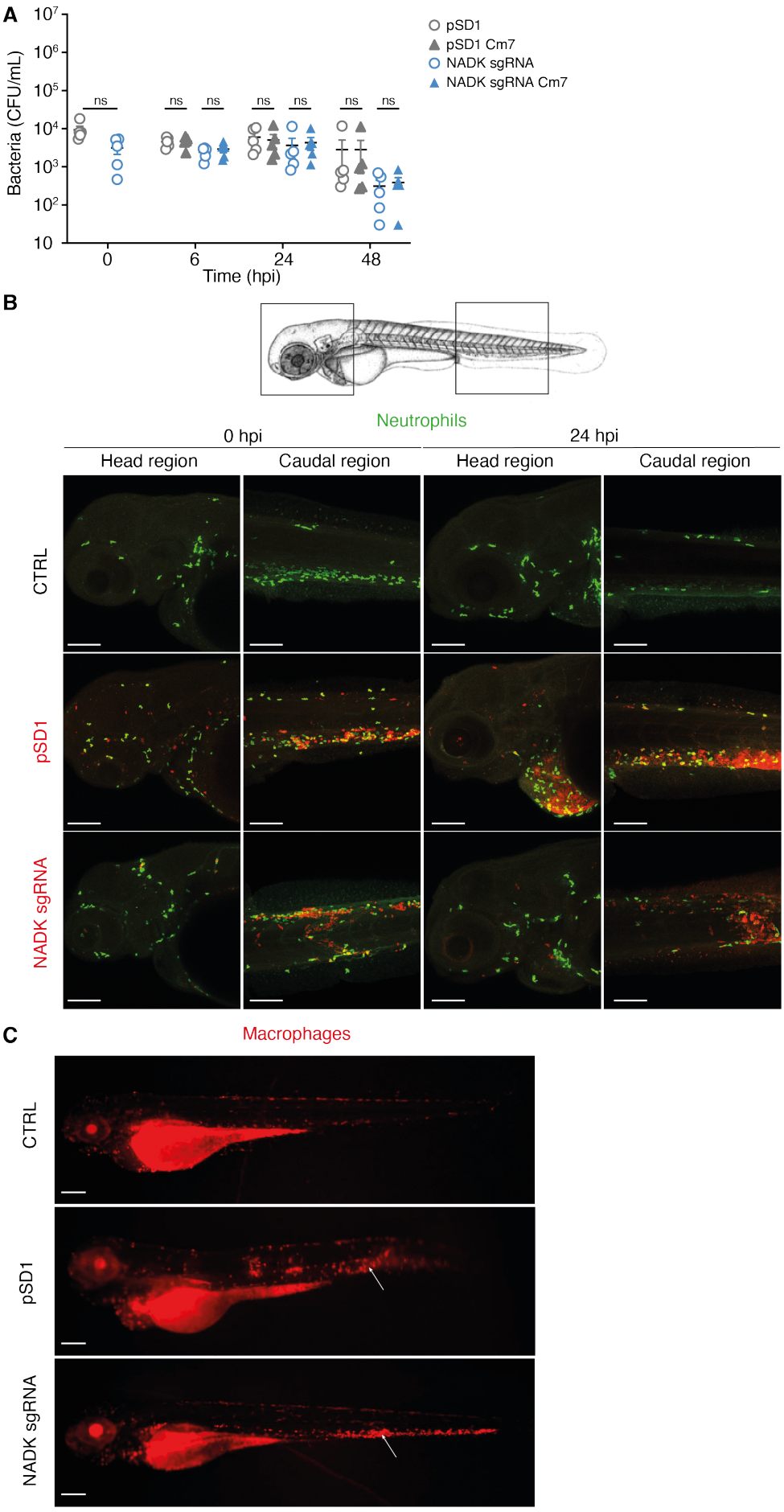
A
Bacteria (CFU/mL)
10^7
10^6
10^5
10^4
10^3
10^2
10
ns
0
6
24
48
Time (hpi)
pSD1
pSD1 Cm7
NADK sgRNA
NADK sgRNA Cm7
B
Neutrophils
0 hpi
24 hpi
Head region
Caudal region
Head region
Caudal region
CTRL
pSD1
NADK sgRNA
C
Macrophages
CTRL
pSD1
NADK sgRNA

1007

1008 **Figure supplement 2** NADK contributes to *S. aureus* virulence in zebrafish. (A) The number of pSD1 (grey) or
1009 NADK sgRNA (blue) *S. aureus* was monitored in zebrafish larvae after intravenous injection with 5.10^3 bacteria.
1010 For each strain, CFU were determined 0, 6, 24 and 48 hpi by plating fish lysates on BHI agar (open circles) and
1011 BHI agar supplemented with chloramphenicol (triangles). (B) Representative fluorescence confocal images of
1012 transgenic *mpx:GFP* zebrafish larvae fixed and labeled with specific antibodies to detect GFP or *S. aureus,*
1013 uninfected (CTRL), or intravenously injected with 10^4 *S. aureus* containing the empty vector (pSD1) or the NADK
1014 knockdown strain (NADK sgRNA) at 0 or 24 hpi. Maximum intensity Z-projection images (2-µm serial optical
1015 sections) of bacteria (red) and neutrophils (green) in the caudal and head regions. Scale bars, 25 µm. (C)
1016 Representative fluorescence confocal images of transgenic *mfap4::mCherryF* zebrafish larvae fixed and labeled
1017 with specific antibodies to detect mCherry or *S. aureus*, uninfected (CTRL), or intravenously injected with 10^4 *S.*
1018 *aureus* containing the empty vector (pSD1) or the NADK knockdown strain (NADK sgRNA) at 24 hpi, showing
1019 macrophages (red). White arrows indicate the injection site. Scale bars, 500 µm.
1020

A

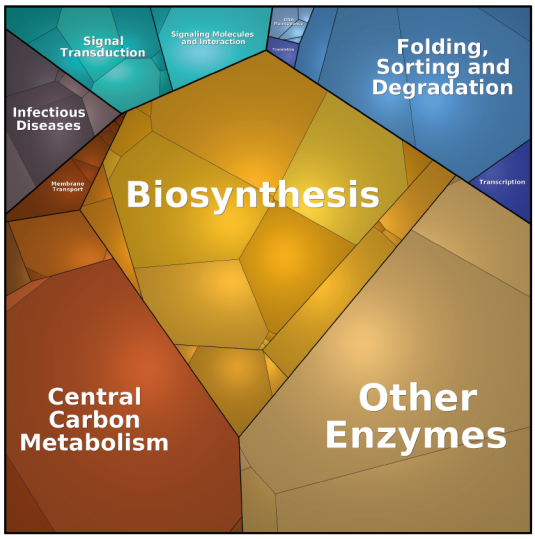
Signal Transduction
Signaling Molecules and Interaction
Folding, Sorting and Degradation
Infectious Diseases
Membrane Transport
Biosynthesis
Transcription
Central Carbon Metabolism
Other Enzymes

B

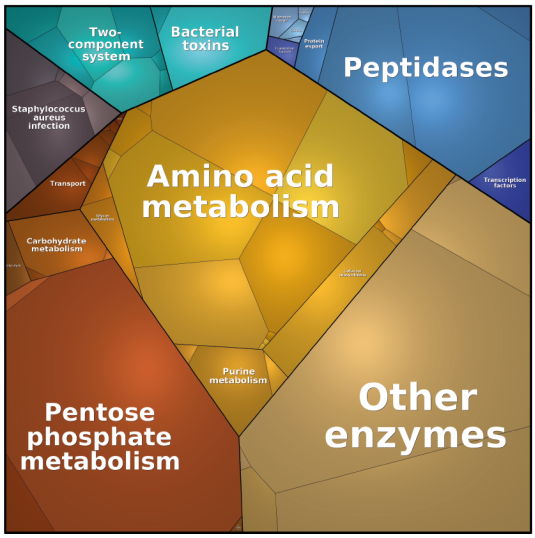
Two-component system
Bacterial toxins
Protein export
Peptidases
Staphylococcus aureus infection
Transport
Amino acid metabolism
Transcription factors
Carbohydrate metabolism
Purine metabolism
Pentose phosphate metabolism
Other enzymes

C

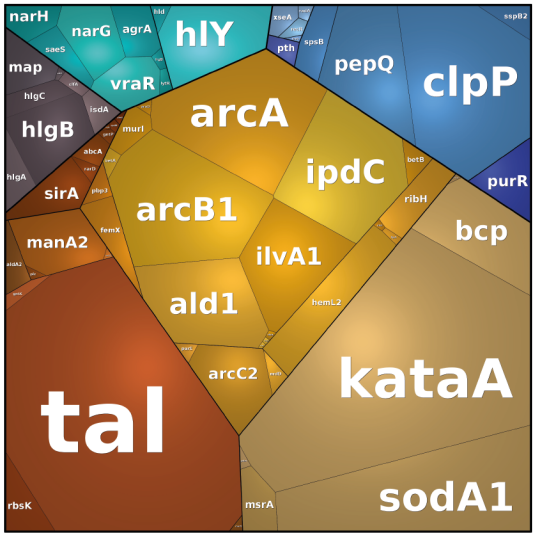
narH
narG
agrA
hlY
xseA
pth
spsB
pepQ
clpP
sspB2
saeS
map
vraR
hlgC
isdA
hlgB
murI
arcA
ipdC
betB
purR
hlgA
sirA
arcB1
ribH
bcp
manA2
femX
ilvA1
ald1
hemL2
arcC2
kataA
tal
rbsK
msrA
sodA1

1021

1022 **Figure supplement 3** NADK promotes expression of *S. aureus* virulence determinants. The *S. aureus* strain
1023 containing the empty vector (pSD1) and the *ppnK* knockdown strain (NADK sgRNA) were grown at 37°C in BHI
1024 broth supplemented with H_2O_2. (A-C) Whole bacterial cell lysates were analyzed by LC-MS/MS. Voronoi
1025 treemaps were generated to visualize proteins more abundant in *S. aureus*/pSD1 than in the knockdown strain at
1026 three hierarchical levels according to KEGG database: top level (A), second level (B), third level (C). Colors
1027 represent functional categories. Category size based on LFQ intensity corresponds to differences in protein
1028 abundance.
1029

1030

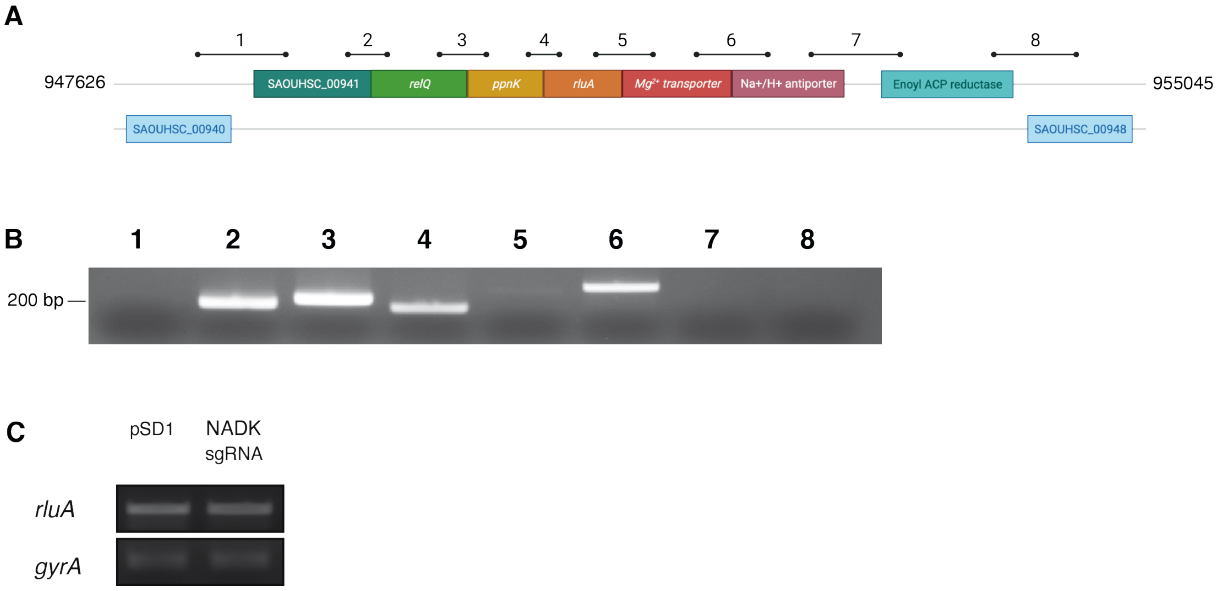

1031

1032

1033 **Figure supplement 4** *S. aureus ppnK* gene is part of the *relQ* operon. (A) Genomic region surrounding the *ppnK*
1034 gene of *S. aureus* Xen36 between nucleotides 947626 and 955045. Bars and numbers represent the regions
1035 amplified by RT-PCR shown in B. (B) Ethidium bromide staining of DNA in an agarose gel following RT-PCR
1036 amplification using total RNA from *S. aureus* Xen36 and primers located in regions indicated in A. (C) Ethidium
1037 bromide staining of DNA in an agarose gel following RT-PCR amplification using total RNA from *S. aureus*
1038 Xen36/pSD1 or Xen36/NADK sgRNA and oligonucleotides specific to the target gene *rluA* or the control gene
1039 *gyrA*, respectively.

1040

1041

1042 **Table supplement 1.** Proteins more abundant in the *S. aureus* pSD1 strain than in the NADK
1043 sgRNA strain after growth in BHI broth (Excel file).
1044
1045
1046 **Table supplement 2.** Relative abundance of a subset of protective proteins differentially
1047 expressed by *S. aureus* pSD1 and NADK sgRNA strains exposed to hydrogen peroxide.
1048

Uniprot	Protein	Description	Log2R*	P**
Q2FV54	OatA	O-acetyl transferase	3.40	6.57E-05
Q2G261	SodM	Superoxide dismutase [Mn/Fe]	2.49	1.66E-07
Q2G000	Trx2	Thioredoxin 2	2.25	1.00E-04
Q2G0E0	GraR	Response regulator protein	2.00	7.15E-06
Q2FZZ3	-	Thioredoxin domain-containing protein	1.86	3.25E-04
Q2G280	-	Peroxiredoxin	1.67	7.37E-08
P0A086	MsrA2	Methionine sulfoxide reductase	1.37	1.27E-04
Q2FYU7	KatA	Catalase	1.17	1.83E-08
Q2FVL7	-	Thioredoxin domain-containing protein	1.02	2.22E-03

1049
1050 * Log2R=Log2[pSD1]/[NADK sgRNA]
1051 **Adjusted p value
1052
1053
1054 **Table supplement 3.** Proteins more abundant in the *S. aureus* pSD1 strain than in the NADK
1055 sgRNA strain after growth in BHI broth supplemented with hydrogen peroxide (Excel file).
1056
1057
1058 **Table supplement 4.** Relative abundance of a subset of protective proteins differentially
1059 expressed by *S. aureus* pSD1 and NADK sgRNA strains upon zebrafish infection.
1060

Uniprot	Protein	Description	Log2R*	P**
Q2G000	-	Thioredoxin domain-containing protein	+	NA
P0A0J3	SodA	Superoxide dismutase [Mn]	+	NA
Q2FYU7	KatA	Catalase	+	NA
Q2FKL3	Tpx	Thiol peroxidase	+	NA
Q2FZW4	DltC	D-alanyl carrier protein	+	NA
O05204	AhpF	Alkyl hydroperoxide reductase subunit F	+	NA
Q2FXI6	-	Thioredoxin domain-containing protein	+	NA
Q2G280	-	Peroxiredoxin	+	NA

1061
1062 * Log2R=Log2[pSD1]/[NADK sgRNA]; +: protein detected in pSD1 strain and not detected from NADK sgRNA strain
1063 **Adjusted p value: NA: not applicable
1064
1065
1066 **Table supplement 5.** Proteins more abundant in the *S. aureus* pSD1 strain than in the NADK
1067 sgRNA strain upon zebrafish infection (Excel file).
1068
1069
1070

1071 **Table supplement 6.** Relative abundance of a subset of virulence-related proteins differentially
1072 expressed by *S. aureus* pSD1 and NADK sgRNA strains exposed to hydrogen peroxide.
1073

Uniprot	Protein	Description	Log2R*	P**
Q2FVK1	HlgB	Gamma-hemolysin component B	+	NA
Q2FWM8	Hld	Delta-hemolysin	+	NA
Q2FWM4	AgrA	Accessory gene regulator protein	+	NA
Q2FVK2	HlgC	Gamma-hemolysin component C	+	NA
P0C818	PsmA4	Phenol-soluble modulin alpha 4	+	NA
P0C7Y1	PsmA1	Phenol-soluble modulin alpha 1	+	NA
Q2FUU5	Lip1	Lipase	+	NA
Q2G1X0	Hly	Alpha-hemolysin	7.99	2.92E-09
Q2FVK3	HlgA	Gamma-hemolysin component A	5.59	1.60E-06
Q2FWP0	LukL1	Leukocidin-like protein 1	3.35	7.16E-06
Q2G2R8	SspP	Staphopain A	3.27	1.17E-06
Q2FWN9	LukL2	Leukocidin-like protein 2	2.98	2.56E-07

1074
1075 *Log2R=Log2[pSD1]/[NADK sgRNA]; +: protein detected in pSD1 strain and not detected from NADK sgRNA strain
1076 **Adjusted p value: NA: not applicable
1077

1078

1079